Production of Heavy Nuclides in 440-MeV Proton Fission of Uranium*

JAMES J. HOGAN† AND NATHAN SUGARMAN
The Enrico Fermi Institute and Department of Chemistry, The University of Chicago, Chicago, Illinois 60637
(Received 15 November 1968)

The recoil properties of 20 nuclides of mass about 140 formed in the 440-MeV proton fission of uranium were determined. The average kinetic energy, cascade deposition energy, and angular anisotropy for each fission product were calculated from the recoil results. The kinetic energy and excitation energy of the primary fragments leading to these fission products, and the total kinetic energy and excitation energy of the primary-fragment pair, were calculated from those of the fission products. The primary-fragment results indicate a dependence of the deformation of the fissioning nucleus on its excitation energy, and explain the trends observed in the kinetic energy and cascade deposition energy of the fission products. The theory used to explain the angular distribution of fission products produced by low-energy (<50 MeV) bombarding projectiles was applied successfully in the explanation of the angular anisotropies observed at 440 MeV. The charge dispersion of the fission products of mass 139 was determined, and was fitted by a Gaussian curve with a full width at half-maximum of 3.2 charge units. The primary fragments leading to isobaric fission products differ from each other by two mass units per charge unit, and are more constant in neutron-to-proton ratio than the fission products.

I. INTRODUCTION

THE complexity of high-energy nuclear fission has thus far precluded a thorough understanding of its mechanism. This reaction has been studied in various ways in an attempt to learn about the fission process by observation of its products. The fast intranuclear cascade leaves a variety of excited nuclei which may fission or deexcite by evaporation of nucleons in competition with fission. The goal of the present work is the study of the recoil properties of fission products in a narrow mass region in order to determine the properties of the primary fission fragments leading to these products. From this, some knowledge of the fission process and its dependence on the division of charge between the two primary fragments is obtained.

Measurements of the recoil properties of fission products have been used previously by many authors to determine kinetic energies, cascade deposition energies, and angular anisotropies for many fission products at many bombarding energies.[1–10] In general, the results show that the kinetic energy of a product is a few percent lower than that observed in thermal neutron fission. The average cascade deposition energy for formation of a product is higher for neutron-deficient products than for neutron-excess ones. The angular distributions generally deviate less than 10% from isotropy. Alexander *et al.*[4] and Brandt[7] observed a dramatic decrease in the range of very neutron-deficient iodine nuclides as the proton bombarding energy increased from 0.5 to 18 GeV, whereas the range of the neutron-excess iodine isotopes remained essentially unchanged. These recoil investigations and the related yield studies of Friedlander *et al.*[11] in the Cs region, Hagebø on Sb,[12] and Dobronrovova *et al.*[13] on Xe nuclides indicate that another production mechanism different from fission is responsible for the formation of the most neutron-deficient species. The present recoil study of *isobaric* fission products, in which the charge rather than the mass dependence of the division of the nucleus is studied, was undertaken to yield information on the dependence of the energetics of the high-energy fission process on charge division.

The exceedingly short lifetimes of the primary fragments preclude the possibility of studying their properties directly. However, the properties of the primary fragments may be calculated from those of the observed fission products by making assumptions regarding the fissionability of the excited cascade nuclei, the division of the total kinetic energy and excitation energy between the two primary fragments, the yield pattern of the primary fragments, and the effect of particle evaporation from the primary fragments on the kinetic energy of the fission products.

In this work, recoil properties of 17 nuclides of atomic number 55 to 60 and mass number 133 to 147 (15 of them in the mass region 138–145) have been measured

* Work supported in part by the U.S. Atomic Energy Commission.

† Submitted in partial fulfillment of the requirements of the Ph.D. degree in the Department of Chemistry of the University of Chicago. The author acknowledges the aid of a Union Carbide Corporation Fellowship. Present address: Department of Chemistry, McGill University, Montreal, Quebec, Canada.

[1] N. Sugarman, M. Campos, and K. Wielgoz, Phys. Rev. **101**, 388 (1956).
[2] N. T. Porile and N. Sugarman, Phys. Rev. **107**, 1410 (1956).
[3] J. B. Niday, Phys. Rev. **121**, 1471 (1961).
[4] J. M. Alexander, C. Baltzinger, and M. F. Gazdik, Phys. Rev. **129**, 1826 (1963).
[5] J. A. Panontin and N. Sugarman, J. Inorg. Nucl. Chem. **25**, 1321 (1963).
[6] V. E. Noshkin and T. T. Sugihara, J. Inorg. Nucl. Chem. **27**, 943 (1965); **27**, 959 (1965).
[7] R. Brandt, in *Physics and Chemistry of Fission* (International Atomic Energy Agency, Vienna, 1965), Vol. II, p. 329.
[8] N. Sugarman, H. Münzel, J. A. Panontin, K. Wielgoz, M. V. Ramaniah, G. Lange, and E. Lopez-Menchero, Phys. Rev. **143**, 952 (1966).
[9] J. A. Panontin and N. T. Porile, J. Inorg. Nucl. Chem. **30**, 2027 (1968).
[10] V. P. Crespo, J. B. Cumming, and A. M. Poskanzer, Phys. Rev. **174**, 1455 (1968).
[11] G. Friedlander, L. Friedman, B. Gordon, and L. Yaffe, P Rev. **129**, 1809 (1963).
[12] E. Hagebø, J. Inorg. Nucl. Chem. **29**, 2515 (1967).
[13] A. N. Dobronrovova, L. K. Levskii, A. N. Murin, and N Titov, Soviet J. At. Energy **14**, 502 (1964).

From these, the momentum transfer to the fissioning nucleus, and the kinetic energy and angular anisotropy of the fission products, have been calculated. These results were used to calculate the identity, kinetic energy, and excitation energy of the average primary fragment leading to each observed product.

The charge dispersion curve for fission products of mass number 139 was determined and found to be symmetric about a most probable charge.

II. EXPERIMENTAL PROCEDURE

A. Measurement of Recoil Properties

The experimental procedure used was similar to that of previous thick-target thick-catcher studies of nuclear reactions performed in this laboratory.[1,2,5,8]

A 1-mil U target foil was surrounded by 1-mil Al catcher foils, and these were enveloped in 1-mil Al foil as shown in Fig. 1. The target stacks for the first experiments on a given element also contained a 1-mil Al foil for impurity activation situated downstream from the target and catchers.

The U foils were of natural isotopic composition, nominally 1-mil thick and 1.0×1.5 cm in size. The surface of the foils was cleaned in dilute hydrochloric acid solution immediately before preparation of the target. The average thickness, ranging from 40 to 43 mg/cm^2, was determined by weighing the target and carefully measuring its size.

The Al catcher foils and envelope were of high-purity (>99.99%) 1-mil Al, more than twice the thickness of the longest-range fission products measured. In no case was there need for an activation correction to the data. The catcher foils were approximately 1.5×2.0 cm so that they overlapped the target by several millimeters on all sides. The envelope was a single sheet of the same high-purity Al, approximately 1×1½ in. in size, folded in such a way that the fold was the leading edge.

Irradiations were performed in the internal beam of the University of Chicago Synchrocyclotron at a radius of 75 in., corresponding to a nominal proton energy of 440 MeV. The period of irradiation varied from 1 min for the short-lived Cs^{139} to 2 h for the long-lived Ce isotopes. The intensity of the proton beam was varied according to the production cross section of the nuclide under investigation, and the volatility of the nuclide and its β-decaying precursors.

Experiments were performed in two orientations, called "parallel" and "perpendicular," as depicted in Fig. 1. The angle of 10° was used in perpendicular experiments to lessen the effects of multiple scattering of the proton beam in what otherwise would effectively be a 1.5-cm-thick target.

After the irradiations, the target package was disassembled and the target and catcher foils were dissolved for radiochemical analysis. The U foils were dissolved in 6*M* HCl in the presence of HNO_3. The

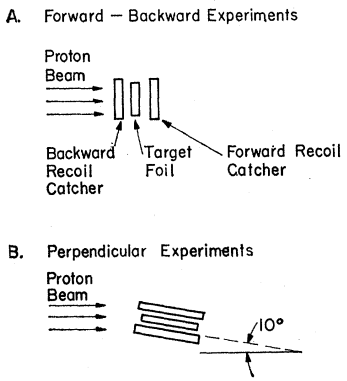

FIG. 1. Target assembly for forward-backward and perpendicular experiments.

Al catcher foils were dissolved in a mixture of 50% 6*M* HCl and 50% 6*M* HNO_3, with heating. In most experiments, the requisite carriers were present in the dissolving solution. The samples were chemically separated by the procedures given in Appendix A, mounted, and counted. The decay curves were generally analyzed after several half-lives of the radioactivities under investigation except for 285-day Ce^{144}, which was counted for 15 months.

B. Measurement of Charge Dispersion

Three ratios of cross sections of nuclides of mass number 139 were measured in order to define an isobaric-charge dispersion curve. These three ratios provide five points to define the parameters of the curve after one cross-section value is used for normalization. The three experiments determined (i) the ratio of the yield of Ba^{139} with no contribution from β-decaying precursors ("independent") to that of Cs^{139} with its full contribution of β-decaying progenitors ("cumulative"), (ii) the ratio of the yield of Ce^{139} (independent) to that of Pr^{139} (cumulative), and (iii) the ratio of the yield of the combined neutron-deficient nuclides to that of the combined neutron-excess nuclides, through a measurement of the ratio of the activity of Ce^{139} (cumulative) to that of Ba^{139} (cumulative). The procedure used in the charge dispersion experiments is given in Appendix B.

The results of these experiments were combined and fitted with a best charge dispersion curve, assumed to be Gaussian. The procedure used was to vary the most probable charge and the full width at half-maximum (FWHM) independently. Each set of assumptions yielded values of the three cross-section ratios. The best fit was then chosen by minimizing the sum of the squares of the deviations of the calculated ratios from the experimental ones.

III. RESULTS AND ANALYSIS OF DATA

A. Charge Dispersion Curve

The relative production cross sections of nuclides of mass 139 were determined by measuring the ratios of

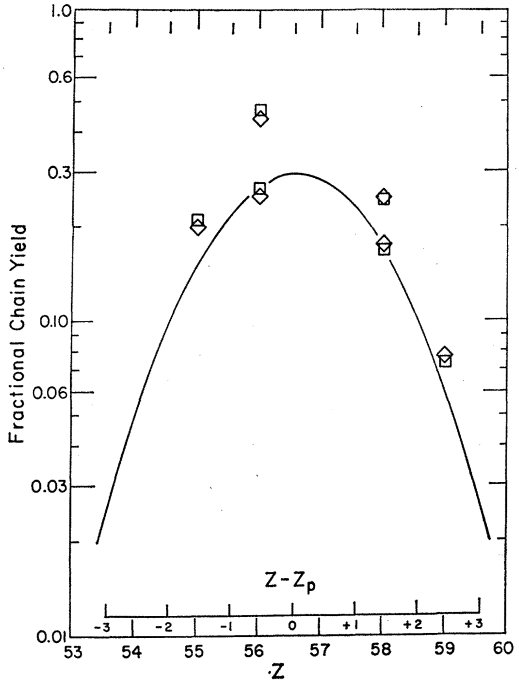

FIG. 2. Charge dispersion curve for fission products of mass 139 □, values predicted from the curve; ◇, experimental values.

the cross section of Cs(C) and Ba(I), Pr(C) and Ce(I), and Ce(C) and Ba(C). Here C stands for "cumulative" and I for "independent," as defined in Sec. II B. The charge dispersion curve for mass 139 was determined from these ratios by assuming a Gaussian curve and determining the parameters which fit the measured ratios best.

The ratio of the cross section of Cs(C) to that of Ba(I) was calculated from the measured activities of the separated Ba fractions as follows. The Cs activity at the time of separation arises from Cs produced directly during the irradiation and from Xe decay during and after the irradiation. The Ba activity at the time of separation results from the Ba produced directly during the irradiation, and from the Cs and Xe decay during and after the irradiation. Three quantities are unknown: the cumulative production cross section for Xe, $\sigma[\mathrm{Xe}(C)]$, the independent ones for Cs and Ba, $\sigma[\mathrm{Cs}(I)]$ and $\sigma[\mathrm{Ba}(I)]$; two quantities are determined: the activities of Ba and Cs at the time of separation.

If one assumes that the ratio $\sigma[\mathrm{Xe}(C)]/\sigma[\mathrm{Cs}(I)]$ is 0.25 (see later discussion and Fig. 2), the Ba activity at the time of separation has less than 0.1% contribution from Xe produced both during and after irradiation. The same assumption permits a direct calculation of the relative cumulative production cross section of Cs from the Cs activity at the time of separation. The activity of Ba at the time of separation was then used to calculate the relative cross section of independent Ba.

The value of the ratio $\sigma[\mathrm{Cs}(C)]/\sigma[\mathrm{Ba}(I)]$ is 0.806±0.029, the error arising from the counting statistics. If the assumption mentioned above is invalid, the error is increased, at most, by 0.016.

The measurement of the ratio $\sigma[\mathrm{Pr}(C)]/\sigma[\mathrm{Ce}(I)]$ was performed in two ways. In the cumulative procedure, three aliquots were taken after 0.1, 1.0, and 12 half-lives of Pr^{139}, and analyzed for Ce^{139} activity. Each of the three samples contained the Ce activity present at the end of irradiation plus that which grew from the decay of Pr prior to the time of separation. The activities of Ce and Pr present at the end of irradiation were calculated by a least-squares analysis of the growth curve of Ce with half-lives of Pr^{139} and Ce^{139} of 4.5 h and 140 days, respectively. After correction for the saturation factors, the ratio $\sigma[\mathrm{Pr}(C)]/\sigma[\mathrm{Ce}(I)]$ was found to be 0.405±0.011.

In the milking experiment, Ce was separated from a single aliquot from the same bombardment as that above after 0.1, 1, and 12 half-lives of Pr^{139}. The last two samples determine the activity of Pr^{139} at the end of bombardment. This value was calculated by a least-squares analysis in which the activity of each sample was weighted by the total number of observed counts. From the milking experiment, a value of the ratio $\sigma[\mathrm{Pr}(C)]/\sigma[\mathrm{Ce}(I)]$ of 0.439±0.009 was calculated.

The cross-section ratio, calculated by weighting the results of the two experiments by the squares of the errors, is 0.426±0.010. It should be noted that this calculation has been performed on the assumption that the half-life of Nd^{139} is short compared to that of Pr^{139} (see Appendix A). Both the growth curve of Ce in the cumulative experiment and the decay of the Ce milked from Pr are consistent with this assumption.

The experiment relating the cumulative yield of neutron-deficient and neutron-excess products was performed by analyses for cumulative Ce and Ba, respectively. After decay of 9.5-min Cs^{139}, Ba was chemically isolated and counted via the same 166-keV transition in La^{139} by which Ce was counted. Because of the decay of Cs to Ba during and after the irradiation, the equation relating the activity measured to the cumulative production cross section contains two unknowns, the cumulative production cross section of Cs and the independent production cross section of Ba. However, the first experiment discussed above relates these and allows direct calculation of the cumulative Ba cross section. The Ce was isolated after 12 half-lives of Pr^{139}. The ratio calculated for $\sigma[\mathrm{Ce}(C)]/\sigma[\mathrm{Ba}(C)]$ is 0.545±0.015, the error arising from the counting statistics.

The cross-section ratios from the three experiments described above are given in Table I. These cross-section ratios may be calculated from a charge dispersion curve assumed to be Gaussian, centered about a selected most probable charge, Z_p, and having a selected FWHM. Calculations were performed for all Z_p values between 56.20 and 56.70, in 0.01 charge unit

TABLE I. Comparison of charge dispersion results with Gaussian-curve analysis.

Cross-section ratio	Observed value	$Z_p=56.58$ FWHM$=3.21$	$Z_p=56.58$ FWHM$=3.41$	$Z_p=56.38$ FWHM$=3.21$
$\sigma[\mathrm{Cs}(C)]/[\sigma[\mathrm{Ba}(I)]$	0.806 ± 0.029	0.785	0.876	0.901
$\sigma[\mathrm{Pr}(C)]/\sigma[\mathrm{Ce}(I)]$	0.426 ± 0.010	0.438	0.515	0.385
$\sigma[\mathrm{Ce}(C)]/\sigma[\mathrm{Ba}(C)]$	0.545 ± 0.015	0.522	0.541	0.373

steps, with FWHM assuming all values between 3.10 and 3.60, in 0.01 charge unit steps. The parameters which give the best fit to the data are Z_p and FWHM equal to 56.58 and 3.21 charge units, respectively. The results of the calculations are given in Table I for the "best-fit" parameters. For comparison, the results for Z_p and FWHM differing by 0.2 charge unit from the "best-fit" values are also given.

A charge dispersion curve giving the fractional chain yield versus charge displacement from Z_p for the nuclides of mass number 139 is given in Fig. 2. The curve is Gaussian in shape, normalized to unity, and has the "best-fit" parameters. A comparison of the measured relative production cross sections for $Cs^{139}(C)$, $Ba^{139}(I)$, $Ba^{139}(C)$, $Ce^{139}(C)$, $Ce^{139}(I)$, and $Pr^{139}(C)$ with those calculated from the charge dispersion curve is also shown. The points derived from the experimental ratios were determined by minimizing the sum of the squares of the deviations of the measured values from those calculated from the curve.

B. Recoil Properties of Fission Products

The recoil properties of the fission products are determined in thick-target thick-catcher experiments from the activity of each of the measured nuclides in the two catchers and in the target foil. The fractions of the activity escaping from the target into the forward and backward catchers are calculated from these quantities, and are called F and B, respectively. In the case of perpendicular experiments, the average fractional activity in each of the two catchers is designated by P. The thickness of the U target, expressed in mg/cm^2, is given by W. The recoil properties characterizing a nuclide are FW, BW, and PW, or combinations of these quantities.

The measured quantities are corrected for two effects[5]: an edge effect arising from recoils escaping from the edges of the target foil, and a scattering effect arising from the net scatter out of the heavy U target into the light Al catchers. For 1-mil U targets bombarded by 450-MeV protons, the correction for the edge effect is taken to be 0.9957 [5] and that for scattering 0.970.[5] The net reduction in the measured activity of fission products in the mass region 140 in the catcher foils is then 3.48% for 1-mil U targets. The recoil properties of each of the nuclides measured, corrected for the edge and scattering effects, are given in Table II. The first column lists the measured nuclide and its mode of formation, cumulative (C), or independent (I), dependent upon the presence or absence in the measured product of significant amounts of activity produced during irradiation as β-decaying precursors. Columns 2 and 3 give the results of the forward-backward experiments and the corresponding standard deviation of the measured average from the true mean. Column 4 gives the number of separate determinations of the forward-backward results on the given nuclide. Column 5 reports the results of the perpendicular experiments and column 6 the number of these experiments on the given nuclide. Values of the recoil properties are given in mg/cm^2 of U.

The recoil parameters of the fission products are calculated from the measured recoil properties on the basis of a two-step model for the high-energy fission process.[14] The first step is the collision of the bombarding particle with the target nucleus, initiating a cascade, and imparting a velocity $\mathbf{v}$ in the laboratory frame, with components $v_{||}$ in the beam direction and $v_\perp$ in a plane perpendicular to the beam. The second step is the fission process, in which a fragment leading to the isolated nuclide is emitted with velocity $\mathbf{V}$ in the system of the struck nucleus. Because of the fast-slow sequence of these events, it is assumed there is no correlation between $\mathbf{v}$ and $\mathbf{V}$. The quantities $\eta_{||}$ and $\eta_\perp$ are defined as $v_{||}/V$ and $v_\perp/V$, respectively.

The range of a product in the laboratory system, $\mathcal{R}$, is taken to be proportional to $\mathcal{U}^N$ where $\mathcal{U}$ is its initial speed and N depends upon the velocity of the product.[4,8] In the moving frame, moving with velocity $\mathbf{v}$, the fission product has a mean range in U, R, proportional to V^N.

The angular distribution of fission products in the moving frame is expressed in the form $a+b\cos^2\theta$, where a and b are constants associated with a given fission product and θ is the angle between the direction of emission of the fission product in the moving frame and the beam direction. A positive value of the anisotropy parameter b/a corresponds to preferential emission along the beam direction, whereas a negative value corresponds to preferential emission in a plane perpendicular to the beam axis.

The equations used to calculate the values of R, $\eta_{||}$,

[14] R. Serber, Phys. Rev. 72, 1114 (1947).

TABLE II. Recoil properties of measured nuclides (corrected).

Nuclide	$2W(F+B)$ (mg/cm²)	$W(F-B)$ (mg/cm²)	Expt	$4WP$ (mg/cm²)	Expt
$Ba^{(133+135)m}(I)$	7.63±0.05	0.401±0.010	3	7.64±0.04	2
$Pr^{138}(I)$	7.00±0.12	0.691±0.054	4	6.76±0.01	3
$Nd^{138}(I)$	6.93±0.13	0.724±0.086	3	6.34±0.07	2
$Cs^{139}(C)$	8.21±0.03	0.096±0.005	7	8.50±0.10	5
$Ba^{139}(C)$	8.15±0.03	0.166±0.009	6	8.38±0.07	5
$Ba^{139}(I)$[a]	8.09±0.07	0.219±0.020		8.30±0.09	
$Ce^{139}(I)$[a]	7.39±0.04	0.450±0.022		7.39±0.16	
$Ce^{139}(C)$	7.34±0.05	0.482±0.024	6	7.30±0.14	4
$Pr^{139}(C)$	7.10±0.09	0.635±0.037	4	6.85±0.02	3
$Ba^{140}(C)$	7.98±0.07	0.192±0.025	5	8.15±0.05	2
$La^{140}(I)$	7.84±0.04	0.387±0.018	3	7.68±0.04	3
$Nd^{140}(I)$	7.08±0.06	0.664±0.054	4	6.86±0.12	2
$Ce^{141}(C)$	7.90±0.07	0.360±0.032	6	8.01±0.09	4
$Pr^{142}(I)$	7.26±0.09	0.398±0.010	4	7.24±0.04	3
$Ce^{143}(C)$	7.86±0.06	0.180±0.022	2	7.95±0.04	2
$Pr^{143}(C)$	7.69±0.08	0.294±0.075	4	7.47±0.06	3
$Pr^{143}(I)$[a]	7.58±0.07	0.363±0.061		7.18±0.05	
$Ce^{144}(C)$	7.62±0.07	0.143±0.041	6	7.73±0.04	4
$Pr^{145}(C)$	7.47±0.08	0.063±0.040	4	7.66±0.01	3
$Nd^{147}(C)$	7.79±0.03	0.094±0.011	4	8.00±0.06	2

[a] Independent values calculated from cumulative values of this nuclide and its β-decaying progenitors using the charge dispersion curve.

$\eta_\perp$, and b/a from the recoil properties if N is taken to be unity (see Sec. III C) are[8,15]

$$2W(F+B)=R\frac{1+\frac{1}{2}b/a+\eta_{||}^2}{1+\frac{1}{3}b/a}, \quad (1)$$

$$W(F-B)=R\eta_{||}, \quad (2)$$

$$4WP=R\frac{1+\frac{1}{4}b/a+\eta_\perp^2(1+\frac{1}{2}b/a)}{1+\frac{1}{3}b/a}. \quad (3)$$

In order to calculate R, $\eta_{||}$, $\eta_\perp$, and b/a from the experimental data, a relationship between $\eta_{||}$ and $\eta_\perp$ is required. This relationship is the same as that of $p_{||}$ and $p_\perp$, the related momenta of the cascade nucleus, shown in Fig. 3 and discussed in Sec. III C.

A computer program was developed to calculate the recoil parameters. As a first approximation, $\eta_{||}$ was taken to be 0.05, $\eta_\perp$ to be 0.0, and b/a to be +0.02. A value of R was calculated from Eq. (1), then a new value of $\eta_{||}$ from Eq. (2), and a value of b/a from the difference of Eqs. (1) and (3). By a process of successive approximation, the three equations were iterated and solved subject to the requirement that the *sum* of the absolute values of the *changes* in R, $\eta_{||}$, and b/a in two successive iterations was not greater than 0.00005.

A preliminary calculation was then made of the kinetic energy by the range-energy equation [Eq. (5)] discussed below. From this the velocity of the fission product, V, the parallel component of the velocity in the moving frame, $v_{||}$, and the parallel momentum imparted to the cascade nucleus, $p_{||}$, were calculated. With the use of the Vegas STEPNO calculation described below, the momentum transferred in the direction perpendicular to the beam, $p_\perp$, was then related to $p_{||}$ (Fig. 3) and a value of $\eta_\perp$ was calculated.

This value of $\eta_\perp$ was then used in a second iteration of the recoil equations with the same procedure as above being followed. The final requirement for the complete solution of the equations was that in two successive iterations, $\eta_\perp$ did not change by more than 0.00005. Thus, the calculation of the recoil parameters yielded results of all four quantities to better than 0.0001.

The results of the calculation of the recoil parameters of the fission products are shown in Table III. The

[15] If N is not equal to unity, the calculated range must be corrected for the effects of the momenta imparted to the system by particle evaporation both before and after fission.

first column shows the measured nuclide and its mode of production. Columns 2–5 are the recoil parameters calculated from Eq. (1)–(3) in the units shown.

C. Kinetic Energy and Cascade Deposition Energy of Fission Products

The kinetic energy of a fission product was calculated by use of the range-energy equation of Lindhard, Scharff, and Schiøtt[16] (LSS), modified from that developed by Bohr.[17] In its most general form, both electronic and nuclear stopping are considered. Noshkin and Sugihara[6] showed that for velocities typical of fission products, the nuclear stopping term can be ignored, and the range-velocity dependence is linear. They fit the range data for thermal neutron fission products stopped in Al,[5,18–23] Zr,[24] Au,[20] and U,[3] to kinetic energy data[25] by the equation

$$\rho(\epsilon) = (1.30/\alpha)\epsilon^{1/2}, \tag{4}$$

where $\rho(\epsilon)$ and ϵ are dimensionless measures of range and energy and α is a parameter which depends upon the mass and charge of the fission product and the stopping material.[16] If only heavy fission products stopped in U are considered, least-squares analysis of the range-energy data results in a slight increase of the proportionality constant of Eq. (4), from 1.30 to 1.312.

After substitution of known quantities into the equation above, the relation used for calculating the kinetic energy as a function of range in U is

$$T = 453.4Z^{7/3}R^2/A(Z^{2/3}+20.4)^3, \tag{5}$$

where Z and A refer to the recoiling nuclide, T is in MeV, and R is in mg/cm^2. In the calculation of the kinetic energy from the range data by Eq. (5), it was assumed that the values of $\langle \mathbf{V} \rangle^2$ and $\langle \mathbf{V}^2 \rangle$ are equal, or that the dispersion of $\mathbf{V}$ is small compared to $\langle \mathbf{V} \rangle^2$. This assumption is indeed valid for neutron-excess fission products both at thermal neutron[19] and GeV proton bombarding energies.[10] It is not valid, however, for neutron-deficient high-energy fission products, *e.g.*, Ba^{131} at 2.2 GeV,[10] where the correction due to the dispersion of $\mathbf{V}$ is about 10% of the kinetic energy. If it is invalid at 440 MeV for neutron-deficient products, the effect would be to increase the reported kinetic energies of these products by a maximum of 5%, or about 2.5 MeV.

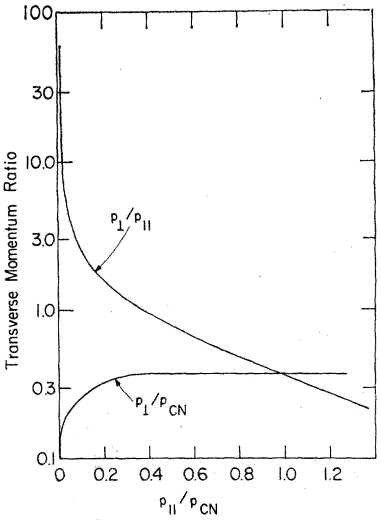

FIG. 3. Relationship of the transverse and parallel components of momentum transferred to the cascade nucleus.

The cascade deposition energy for production of a given fission product was determined by combining the results of the recoil experiments with those of calculations performed at Brookhaven National Laboratory. Using the Vegas STEPNO formalism,[26] 2500 cascades for 380-MeV protons impinging on U^{238} were carried out. The output of this calculation includes the Z and A of the cascade nucleus, its excitation energy, the parallel and perpendicular momentum components relative to the beam direction, and the total angular momentum imparted to the cascade nucleus as well as its projection along the beam axis.

The average momentum transferred to the cascade nucleus along the beam direction, p_{II}, was calculated for each of several intervals of deposition energy. Figure 4 shows the relation between p_{II}/p_{CN} and E^*/E^*_{CN} derived from these calculations. The quantities p_{CN} and E^*_{CN} are the momentum and excitation energy, respectively, which the target nucleus would have if a compound nucleus (CN) had been formed. The momentum and excitation energy transfer are expressed as fractions of the corresponding CN values in order to apply the results of the Vegas STEPNO calculation for 380-MeV protons to the analysis of the 440-MeV proton experiments reported here. Vertical error bars in Fig. 4 represent the width of the E^*/E^*_{CN} bins chosen from the Vegas data. Horizontal bars represent the standard deviation of the average p_{II}/p_{CN} values about the mean. The relationship between these quantities was determined by a least-squares analysis over

[16] J. Lindhard, M. Scharff, and H. E. Schiøtt, Kgl. Danske Videnskab. Selskab, Mat.-Fys. Medd. **33**, No. 14 (1963).
[17] N. Bohr, Phys. Rev. **59**, 270 (1941).
[18] N. K. Aras, Ph.D. thesis, MIT, 1964 (unpublished).
[19] F. Brown and B. H. Oliver, Can. J. Chem. **39**, 616 (1961).
[20] J. M. Alexander and M. F. Gazdik, Phys. Rev. **120**, 874 (1960).
[21] F. Suzor, Ann. Phys. (N.Y.) **4**, 269 (1949).
[22] N. Sugarman, J. Chem. Phys. **15**, 544 (1947).
[23] B. Finkle, E. J. Hoagland, S. Katcoff, and N. Sugarman, in *Radiochemical Studies: The Fission Products*, edited by C. Coryell and N. Sugarman (McGraw-Hill Book Co., New York, 1951), Nat. Nucl. Energy Ser., Vol. IV-9, p. 471.
[24] B. G. Harvey, Ann. Rev. Nucl. Sci. **10**, 235 (1960).
[25] J. C. D. Milton and J. S. Frazer, Can. J. Phys. **40**, 1626 (1962).
[26] K. Chen, Z. Fraenkel, G. Friedlander, J. R. Grover, J. M. Miller, and Y. Shimamoto, Phys. Rev. **166**, 949 (1968).

TABLE III. Recoil parameters of measured nuclides.

Nuclide	R (mg/cm^2)	$\eta_\parallel$	$\eta_\perp$	b/a
$Ba^{(133+135)m}(I)$	7.62±0.05	0.053±0.001	0.056±0.002	−0.007±0.036
$Pr^{138}(I)$	6.81±0.12	0.102±0.008	0.066±0.005	0.113±0.074
$Nd^{138}(I)$	6.50±0.12	0.111±0.013	0.068±0.008	0.367±0.100
$Cs^{139}(C)$	8.40±0.03	0.011±0.001	0.035±0.002	−0.126±0.047
$Ba^{139}(C)$	8.30±0.03	0.020±0.001	0.041±0.002	−0.109±0.034
$Ba^{139}(I)$[a]	8.22±0.07	0.027±0.002	0.045±0.004	−0.097±0.052
$Ce^{139}(I)$[a]	7.37±0.04	0.061±0.003	0.060±0.003	−0.009±0.090
$Ce^{139}(C)$	7.29±0.05	0.066±0.003	0.062±0.003	0.014±0.080
$Pr^{139}(C)$	6.90±0.08	0.092±0.005	0.065±0.004	0.129±0.053
$Ba^{140}(C)$	8.08±0.07	0.024±0.003	0.044±0.006	−0.083±0.043
$La^{140}(I)$	7.72±0.04	0.050±0.002	0.056±0.003	0.082±0.030
$Nd^{140}(I)$	6.90±0.06	0.096±0.008	0.065±0.005	0.106±0.080
$Ce^{141}(C)$	7.96±0.07	0.045±0.004	0.054±0.005	−0.058±0.053
$Pr^{142}(I)$	7.23±0.08	0.055±0.001	0.060±0.002	0.008±0.052
$Ce^{143}(C)$	7.92±0.06	0.023±0.003	0.045±0.005	−0.042±0.035
$Pr^{143}(C)$	7.53±0.07	0.039±0.010	0.053±0.014	0.121±0.052
$Pr^{143}(I)$[a]	7.30±0.07	0.050±0.008	0.058±0.010	0.237±0.052
$Ce^{144}(C)$	7.69±0.07	0.019±0.005	0.043±0.012	−0.057±0.043
$Pr^{145}(C)$	7.59±0.08	0.008±0.005	0.035±0.022	−0.092±0.040
$Nd^{147}(C)$	7.92±0.03	0.012±0.001	0.037±0.004	−0.096±0.031

[a] Independent values calculated from cumulative values of this nuclide and its β-decaying progenitors using the charge dispersion curve.

two momentum regions in each of which a linear dependence was used.

$$E^*/E^*_{CN}=0.860(p_{||}/p_{CN})-0.008, \quad p_{||}/p_{CN}<0.56 \tag{6}$$

$$E^*/E^*_{CN}=1.136(p_{||}/p_{CN})-0.164, \quad p_{||}/p_{CN}>0.56. \tag{7}$$

The quantity $p_{||}/p_{CN}$ was approximated by $v_{||}/v_{CN}$.

A relationship was also derived relating the average momentum transferred to the cascade nucleus in the plane perpendicular to the beam direction, $p_\perp$, to that parallel to the beam direction, $p_{||}$. Figure 3 shows this relationship plotted in two ways. The perpendicular momentum imparted to the struck nucleus and the ratio of the perpendicular to the parallel component are both shown as a function of the parallel component. The plots have been derived in the same manner as that above for the relationship of parallel momentum to excitation energy deposited, and are plotted, similarly, in terms of the ratio of the momentum transferred to that expected if a compound nucleus were the result of the cascade interaction. The value of $p_\perp/p_{CN}$ as a function of $p_{||}/p_{CN}$ may be expressed as

$$\ln(p_\perp/p_{CN})=0.287\ln(p_{||}/p_{CN})-0.706, \quad p_{||}/p_{CN}<0.4 \tag{8}$$

$$p_\perp/p_{CN}=0.382, \quad p_{||}/p_{CN}>0.4. \tag{9}$$

It should be noted that while the ratio of the perpendicular to the parallel momentum transfer rapidly decreases with increasing values of the parallel momentum transfer, the perpendicular momentum transfer is itself increasing from zero to a constant value.

Calculation of the kinetic energy of a cumulative fission product requires knowledge of the average charge of the recoiling nuclide. This quantity is calculated by making use of the charge dispersion curve (Fig. 2), and the most probable charge at each mass number, Z_p. Table IV shows the value of Z_p at each mass number for which a cumulative fission product was measured. The value at mass 139 was determined directly; the value at each of the other masses was taken from the work of Sugarman *et al.*[8] and that of Pappas and Hagebø[27] and will be discussed in detail in Sec. IV A (Fig. 5).

[27] A. C. Pappas and E. Hagebø, J. Inorg. Nucl. Chem. 28, 1769 (1966).

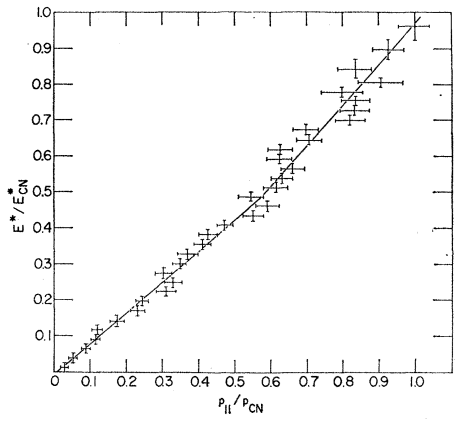

FIG. 4. Dependence of the fraction of the proton bombarding energy transferred to the cascade nucleus on the fraction of the proton momentum transferred to the cascade nucleus.

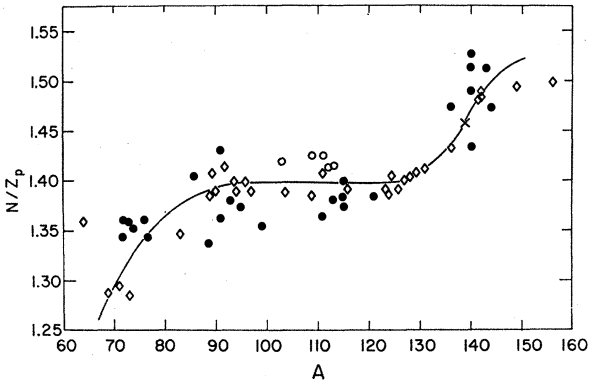

FIG. 5. Variation of the ratio of the neutron number to most probable charge, N/Z_p, with mass number A. ●, work of Sugarman *et al.* (Ref. 44); ◇, work of Pappas and Hagebø (Ref. 27); ○, work of Panontin and Porile (Ref. 39); ×, this work.

The equation taken for the fractional-yield curve for the heavy masses is

$$y_i = 0.294 \exp[-(Z_i - Z_p)^2/3.716], \qquad (10)$$

corresponding to a FWHM of 3.21 charge units (Sec. III A).

The results of the calculation of the kinetic energy and cascade deposition energy of the fission products are shown in Table V, and Figs. 6 and 7. The first column shows the measured nuclide and its mode of production. The next column gives the average value of Z, $\langle Z\rangle$, used in the kinetic energy equation. In the case of an independently measured nuclide, $\langle Z\rangle$ is that of the nuclide itself. For a cumulative product, the $\langle Z\rangle$ value is that calculated by using the fission-product charge dispersion curve [Eq. (10)], a Z_p value from Table IV, and calculating a weighted average of Z over the β-decaying precursors. Column 3 shows the kinetic energy calculated from Eq. (5). Column 4 gives the cascade deposition energy E^* calculated from the results of the Vegas STEPNO calculation [Eq. (6) and (7)]. The final column gives the value of $\langle N\rangle/\langle Z\rangle$, the ratio of the average number of neutrons to the average number of protons in the observed fission product. In the case of an independently produced nuclide, it is N/Z of the nuclide itself. The errors listed in columns 3 and 4 are the standard deviations of the average values of the calculated quantities from the true means.

A cursory examination of the results of Tables III and V indicates the following trends, which will be discussed in detail in Sec. IV: With decreasing neutron-to-proton ratio, the range, and therefore the kinetic energy, decrease approximately 17% and 30%, respectively (Fig. 6); the excitation energy deposited in the

TABLE IV. Values of Z_p used in this work.

Mass number	Z_p	Mass number	Z_p
139	56.58	144	57.60
140	56.63	145	57.88
141	56.81	147	58.46
143	57.31		

TABLE V. Kinetic energy and cascade deposition energy of measured nuclides.

Nuclide	$\langle Z\rangle$	T (MeV)	E^* (MeV)	$\langle N\rangle/\langle Z\rangle$
$Ba^{(138+135)m}(I)$	56.0	54.7±0.8	128±4	1.398
$Pr^{138}(I)$	59.0	45.9±1.6	229±19	1.339
$Nd^{138}(I)$	60.0	42.9±1.6	247±29	1.300
$Cs^{139}(C)$	54.7	61.9±0.5	26±2	1.541
$Ba^{139}(C)$	55.4	61.7±0.6	48±3	1.509
$Ba^{139}(I)$	56.0	61.5±1.1	66±6	1.482
$Ce^{139}(I)$	58.0	52.1±0.6	143±7	1.396
$Ce^{139}(C)$	58.2	51.2±0.7	153±8	1.388
$Pr^{139}(C)$	59.2	47.8±1.2	206±13	1.348
$Ba^{140}(C)$	55.4	58.1±1.0	56±8	1.527
$La^{140}(I)$	57.0	55.3±0.6	120±6	1.456
$Nd^{140}(I)$	60.0	47.7±0.8	216±18	1.333
$Ce^{141}(C)$	56.5	57.6±1.0	109±10	1.496
$Pr^{142}(I)$	59.0	50.3±1.2	125±4	1.407
$Ce^{143}(C)$	56.8	56.6±0.8	52±7	1.518
$Pr^{143}(C)$	58.2	53.2±1.1	89±24	1.457
$Pr^{143}(I)$	59.0	50.9±1.0	112±20	1.424
$Ce^{144}(C)$	57.0	53.3±1.0	41±13	1.526
$Pr^{145}(C)$	57.6	52.4±1.0	16±12	1.517
$Nd^{147}(C)$	58.3	57.4±0.5	25±4	1.521

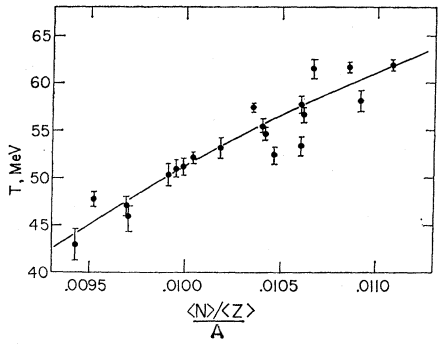

FIG. 6. Dependence of the fission-product kinetic energy T on the ratio of the average neutron number to average proton number, divided by the mass number $(\langle N\rangle/\langle Z\rangle)/A$.

target nucleus increases from near zero to about 60% of the full 440 MeV available (Fig. 7); and the anisotropy parameter increases from negative values, through zero, to positive values (Fig. 8).

IV. DISCUSSION OF PROPERTIES OF FISSION PRODUCTS

A. Charge Dispersion in High-Energy Fission

The most probable charge Z_p at each mass is a necessary parameter in determining the average charge of an observed cumulative fission product. In order to calculate a value of Z_p at each mass, a plot of N/Z_p versus A was obtained in the following manner. Sugarman *et al.*[8] and Panontin and Porile[9] have reported values of N/Z_p for observed fission products from 450-MeV fission of U, and N/Z_p at mass 139 was determined in this work. To define the curve further, the quite extensive data measured and collected by Pappas and Hagebø[27] at 170 MeV were corrected for the difference in bombarding energies. This correction was made using the average value from Sugarman *et al.*[8] of the cascade deposition energy leading to the product of most probable charge at a given mass, and the plot from Pappas and Hagebø[27] of the average number of

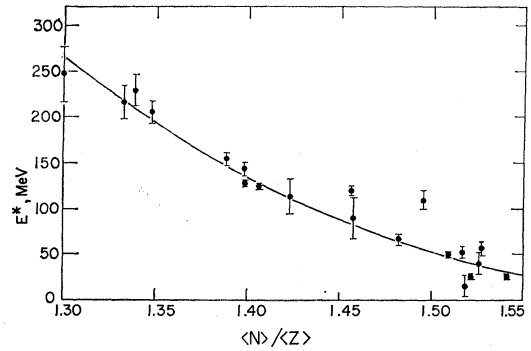

FIG. 7. Dependence of the cascade deposition energy E^* on the ratio of the average neutron number to average proton number $\langle N\rangle/\langle Z\rangle$.

evaporated neutrons associated with the production of each fission-product mass. With the assumption that 10 MeV is required to evaporate a neutron, the plot of Pappas and Hagebø was converted to a plot of average deposition energy for each given mass. It was then assumed that a product of charge Z_p observed in 170-MeV fission by Pappas and Hagebø would have been observed by Sugarman *et al.* in 450-MeV fission at a different mass, because of the increased neutron evaporation at the higher bombarding energy.

The increase in the number of neutrons evaporated at the higher bombarding energy was calculated and used to adjust the data of Pappas and Hagebø to the higher bombarding energy. The effect is to move the points of Pappas and Hagebø to lower values of A and correspondingly lower values of N/Z_p.

The data of Sugarman *et al.*,[8] Panontin and Porile,[9] Pappas and Hagebø,[27] and the value at mass 139 measured in this work are plotted in Fig. 5. This curve has

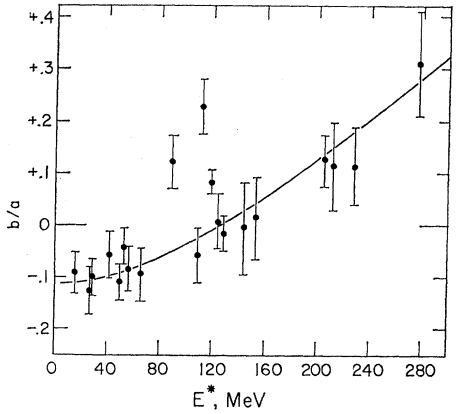

FIG. 8. Variation of the anisotropy factor b/a with cascade deposition energy E^*.

been used to determine the values of Z_p at each mass of interest in this work (Table IV). The average charge of a cumulative fission product is calculated by use of the charge dispersion curve, Eq. (10).

An apparently serious discrepancy had arisen between the previously published work of Friedlander *et al.*[11] (FFGY) and Sugarman *et al.*[8] on the width of the fission-product charge dispersion curve at about 400 MeV. In FFGY, the production cross sections for many nuclides of mass number about 135 are plotted against the neutron-to-proton ratio of the observed product. It was concluded from this plot that for 380-MeV protons the charge dispersion had a FWHM of 5.2 charge units. On the other hand, work of Sugarman *et al.*, based on data in the mass region above $A=100$, indicated that FWHM was about 3.5 charge units in the same mass region.

This apparent discrepancy has now been explained in part. Friedlander *et al.* determined the charge dispersion width from their cross-section data by assum-

ing that the most probable neutron-to-proton ratio N/Z_p is constant over the mass region studied. However, as seen in Fig. 5 and discussed above, this is probably not the case. While the ratio N/Z_p appears to be constant from about mass 95 to 120, it is apparently increasing at higher masses. The values of N/Z_p from Fig. 5 allow calculation of Z_p at each mass studied by FFGY.

A charge dispersion curve was calculated from the FFGY[11] cross sections for independent nuclides corrected for the variation in the total chain yield with mass reported for 340-MeV fission by Folger *et al.*[28] The resultant data were fitted to a normalized Gaussian-shaped curve and are shown in Fig. 9 as the fractional chain yield versus displacement of charge from the most probable. The FWHM of the fractional chain yield curve is 3.0 charge units, in good agreement with Folger, Stevenson, and Seaborg[28] at mass 140 (3.0 charge units), Sugarman *et al.*[8] in the heavy mass region (3.5 charge units), Panontin and Porile[9] in the symmetric fission region (2.9 charge units), Hagebø[12] in mass region 130 for 580-MeV fission (3.2 charge units), and this work at mass 139 (3.2 charge units). However, a serious difference still remains between the cross sections of three cumulative nuclides measured by FFGY and those which would be predicted on the basis of the charge dispersion curve of Fig. 9.

There is also an apparent discrepancy in FWHM, in the region of bombarding energy around 150 MeV, between the values found by Pappas and Hagebø[27] in mass chains 127–134 for 170-MeV fission (FWHM of 2.8 charge units) and those found by FFGY[11] at 100 MeV (3.3 charge units) and 200 MeV (3.8 charge units). Pappas and Hagebø showed that the value of N/Z_p in this region increases from 1.458 to 1.481. If their data are plotted against N/Z, and N/Z_p is assumed to be constant, the apparent FWHM increases from 2.8 to 3.4 charge units. The peak in the N/Z plot so drawn is at a value of 1.480 in excellent agreement with the average value from FFGY of 1.478. The FWHM results are thus consistent; in this case, too, the apparent discrepancy in the FWHM values arises from the FFGY assumption of constant N/Z_p over the mass region.

If the fractional chain yield curve of Fig. 9 is normalized at Cs^{134} to the cross section observed by FFGY, the cross sections for the ten other independent and three cumulative cross sections may be calculated. The 11 independent cross sections are reproduced with an average deviation from the experimental values of less than 0.5 mb. The cumulative cross sections of Cs^{135}, Cs^{137}, and Ba^{140} are not reproduced well, being underestimated in each case by a factor of about 2, as shown in Fig. 9. In order to reproduce the cumulative data, a much flatter, though not necessarily broader, non-Gaussian shaped charge dispersion curve is required.

[28] R. L. Folger, P. C. Stevenson, and G. T. Seaborg, Phys. Rev. **98**, 107 (1955).

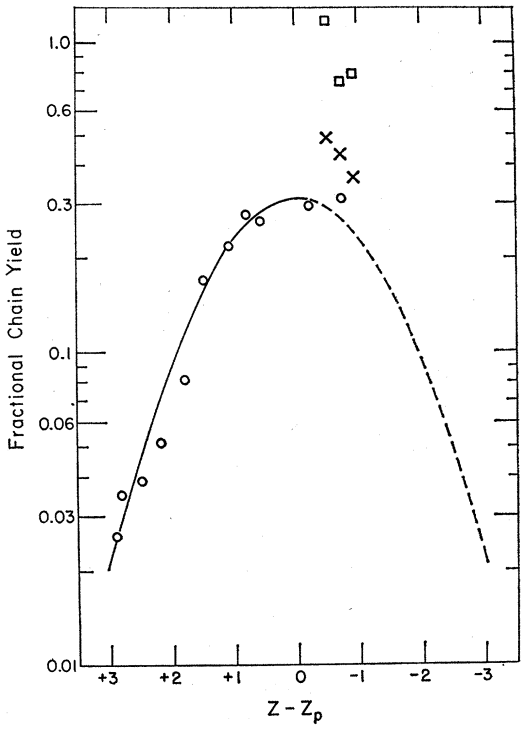

FIG. 9. Charge dispersion curve for fission products of mass 126–140. The data are taken from Friedlander *et al.* (Ref. 37), reanalyzed as discussed in Sec. IV A. ○, data of Friedlander *et al.*, independent nuclides; □, data of Friedlander *et al.*, cumulative nuclides; ×, values for cumulative nuclides predicted from the curve. The curve has been reflected (dashed line) about the most probable charge.

B. Energetics of Production of Observed Fission Products

1. Kinetic Energy of Fission Products

The calculation of the kinetic energy of a fission product from its experimental range was carried out using a modified form of the Lindhard, Scharff, and Schiøtt[16] theoretical treatment of the stopping of heavy ions. Both electronic and nuclear stopping are considered in the general formulation; however, since the nuclear stopping term is estimated to account for only 10% of the total stopping even after the fission-product kinetic energy has been reduced by about 70%,[29] it may be ignored in dealing with fission products.

The agreement between the Lindhard *et al.*[16] universal stopping theory and experimental data is good.[29] However, quantitative disagreements do exist, the prime one of interest in this work being an underestimate of the stopping power for high-velocity atoms, and therefore an overestimate of the range of fission products, particularly the light ones. Various parameters have been used[18,29–31] to normalize the predictions

[29] J. B. Cumming and V. P. Crespo, Phys. Rev. **161**, 287 (1967).
[30] J. Lindhard and M. Scharff, Phys. Rev. **124**, 128 (1961).
[31] C. D. Moak and M. D. Brown, Phys. Rev. **149**, 244 (1966).

of the Lindhard *et al.* theory to existing experimental data. In particular, Noshkin and Sugihara[6] showed that agreement between experiment and theory over a wide range of fission products and stopping materials could be obtained by a 35% reduction in the proportionality constant relating range and velocity. The range data of Niday[3] and kinetic energy data of Milton and Fraser[25] were used to determine the constant of Eq. (5) used in this work.

Other forms of the range-energy equation have been used, such as that due to Panontin and Sugarman[5] and to Alexander *et al.*,[32] namely, $R=CT^N$, in which C and N are parameters depending upon the mass of the stopping and recoiling atoms. This form of the range-energy dependence does not, however, include an explicit dependence on the charge of the recoiling atoms of a given mass, a quantity of great interest in this work. Use of the Panontin and Sugarman[5] range-energy formalism, including their correction for the average charge of the recoiling atom, would increase the values reported here for the kinetic energy 3–5%, and slightly increase the slope of the dependence of the kinetic energy on the neutron-to-proton ratio of the fission products.

Besides the experimental work cited in Sec. III C,[3,5,18–24] which can be adequately described by an equation in which the range varies linearly with velocity, several other authors[29,33–36] have reported data supporting this dependence. The work of Cumming and Crespo[29] on fission products recoiling through Mylar shows experimental points on a range-velocity plot deviating only slightly from linearity over the velocity range of interest in this work. A better fit to the data was obtained by variation of the dependence of the range on the charge of the recoiling atom as a function of velocity. Over the narrow region of velocities encountered in this work, this variation was not used. Other work[33–36] also reports experimental data showing a linear dependence of range on velocity within experimental error, and excellent fits to the predictions of the LSS theory result after various adjustments are made in the proportionality constant described above. In the present work, the intercept of the range-velocity curve was taken to be zero, consistent with ignoring the nuclear stopping term.

The results of the calculations of the average kinetic energy of observed fission products are shown in Table V and plotted in Fig. 6. The abscissa $(\langle N\rangle/\langle Z\rangle)/A$ was used in order to reduce the effect of the A dependence of kinetic energy in this region. The average range decreases with increasing A over the mass region from 130 to 150,[3,8] with approximately a $1/A$ dependence. Therefore, the variation of the observed kinetic energy with the average neutron to average proton ratio divided by A should more nearly represent the isobaric kinetic energy dependence. It should be noted, however, that introduction of this $1/A$ dependence does not substantially alter the kinetic energy curve; the scatter is slightly reduced.

A 17% decrease in the range of the observed fission products from the most neutron-excess to the most neutron-deficient has been observed. This corresponds to a decrease of ~30% in the kinetic energy from the most neutron-excess product measured Cs^{139} to the most neutron-deficient Nd^{138}. A reduction in the kinetic energy of less neutron-excess fission products was first observed in the thermal neutron fission work of Niday.[3] The range measured for each of the two "shielded" nuclides, Rb^{86} and Cs^{136}, lying near β stability, was 10% lower than the average range for neighboring mass chains, as was confirmed by Brown and Oliver[19] in the case of Cs^{136}. Hollstein[37] measured the ranges of independently produced nuclides of mass number 139 from thermal neutron fission of Pu^{239} and found a nearly linear decrease of the kinetic energy with increasing Z of the fission product, about 7% per charge unit.

Nakahara[38] explained the short range of the shielded nuclide, Cs^{136} by its formation from processes involving primary fragments with considerably higher than average excitation energies and lower than average kinetic energies. In the case of thermal neutron fission, where the total energy of the fissioning nucleus is constant, the kinetic and excitation energies are directly related to each other.

The case of high-energy fission is more complex since the fissioning nucleus does not have a constant mass charge and excitation energy. The effect of these quantities on the fission process and the primary fragments is discussed in Sec. V B. The interpretation of the ~30% decrease in the kinetic energy of the most neutron-deficient fission products relative to the most neutron-excess ones is based on the calculation of the primary fragments and is given later in Sec. V C.

The kinetic energy of the nuclides of mass 139 and 140 is plotted versus $\langle Z\rangle - Z_p$ in Fig. 10. There is a linear dependence in the variation of kinetic energy with $\langle Z\rangle$, with a slope of ~3.0 MeV, or about 6%, per charge unit. It is interesting to note that this value is nearly the same as that observed by Hollstein[37] in the mass 139 chain from thermal neutron fission, about 7% per charge unit. In the light of later discussion on the source of the kinetic energy reduction in the neutron-deficient products from high-energy fission, it must be concluded that this agreement is probably fortuitous.

It is of considerably greater significance that over the broad range of charge studied for a given mass, no

[32] J. M. Alexander, M. F. Gazdik, A. R. Trips, and S. Wasif, Phys. Rev. **129**, 2659 (1963).
[33] M. Kaplan and P. Richards, Phys. Rev. **145**, 153 (1966).
[34] V. Subrahmanyan and M. Kaplan, Phys. Rev. **142**, 174 (1966).
[35] M. Kaplan and R. D. Fink, Phys. Rev. **134**, 30 (1964).
[36] J. Gilat and J. M. Alexander, Phys. Rev. **136**, 1298 (1964).
[37] M. Hollstein, Ph.D. thesis, Kernforschungzentrum, Karlsruhe, 1965 (unpublished.)
[38] H. Nakahara, Ph.D. thesis, MIT, 1966 (unpublished).

significant deviation from linearity in the kinetic energy dependence on $\langle Z \rangle$ is observed. There is no indication of a discontinuity occurring in the kinetic energy of the very neutron-deficient nuclides. This is in marked contrast to the results[4,7,9,10] of studies carried out at multi-GeV energies, where a marked reduction was observed in the kinetic energy of the neutron-deficient products as the bombarding energy increased into the GeV region. This effect has been attributed to a process other than binary fission which becomes important only at high energies.

2. *Cascade Deposition Energy Leading to an Observed Product*

To cascade deposition energy associated with the production of a fission product is determined from the measured recoil results by use of Eqs. (1)–(3), as discussed in Sec. III C. The momentum transferred to the cascade nucleus along the beam direction, $p_{||}$, is calculated from $\eta_{||}$ after determination of the velocity of the fission product, V, from the range-energy equation. The relation between $p_{||}$ and the excitation energy deposited in the cascade nucleus is obtained from the intranuclear cascade calculations.

The calculation used in this work was the Vegas[26] calculation performed for 380-MeV protons impinging on U^{238}, with no account taken of pion production. Although the distribution of the cascade nuclei in Z and A was taken directly from the calculation, the cascade deposition energy and the linear momentum transferred to the cascade nucleus were corrected for the difference in bombarding energy. The correction was made on the assumption that the ratio of the cascade deposition energy to that expected for compound nucleus production, E^*/E^*_{CN}, and the ratio of the linear momentum transfer to that expected for compound-nucleus production, $p_{||}/p_{CN}$, were the same at 380 and 440 MeV.

Two forms of the Vegas calculation are available, called STEP and STEPNO,[26] corresponding to inclusion or neglect of refraction and reflection at the nuclear potential boundaries between successive radial steps. The STEPNO calculation was chosen on the basis of better agreement between calculated and experimental cross-section results for high Z targets.[26]

In this section, only the excitation energy-linear momentum relationship of the cascade nucleus will be considered. This relationship is ambiguous since it is possible to calculate the average momentum transfer for a given region of excitation energy deposited, and the average value of excitation energy for a given momentum transfer. The choice between the two relationships was made by considering the deposition energy to be the crucial point in determining the identity of the final product. That individual fission products "select out" cascade events with certain values of the deposition energy was discussed in detail by Sugarman

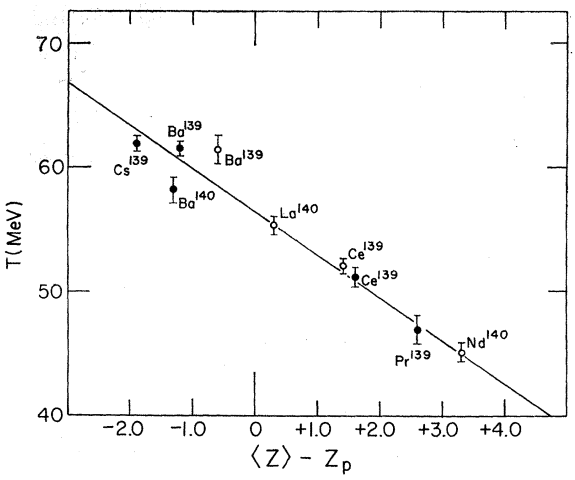

FIG. 10. Isobaric dependence of the fission-product kinetic energy T on the displacement of the average fission-product charge from the most probable charge for mass chains 139 and 140. ○, independently formed nuclides; ●, cumulatively formed nuclides.

et al.[8] For example, Ba^{140} is produced from cascades with 50–60 MeV of deposition energy, independent of the bombarding energy: 170 MeV,[6] 450 MeV,[8] or 2.2 GeV.[10] It was decided, therefore, to calculate as in earlier work the average momentum transfer parallel to the beam, having "selected out" all events leading to a given cascade deposition energy. The relationship derived is that given in Fig. 4, and the data were fitted to straight lines over two regions of E^*/E^*_{CN}, Eqs. (6) and (7).

The average deposition energy of the cascade nucleus leading to an observed product (Table V) is related to the ratio of the average neutron number to average proton number of the product as shown in Fig. 7. The values of the average proton number $\langle Z \rangle$ are listed in Table V. The increase in excitation energy required to produce neutron-deficient fission products had been observed previously by Alexander *et al.*[4] and Sugarman *et al.*[8] The general interpretation of these results is that more excitation energy is required to evaporate enough particles (nearly all neutrons in this mass and excitation energy region) to produce neutron-deficient species from the normally neutron-excess primary fragments. This interpretation has been supported and discussed in detail by Sugarman *et al.*[8] who analyzed the data of several authors,[4,6,8,11] using the procedure of Porile and Sugarman,[2] and arrived at two conclusions. First, the production of neutron-deficient nuclides requires large amounts of cascade deposition energy, as shown by their sharply increasing excitation functions with increasing bombarding energy (up to GeV energies). This is in contrast with the excitation functions of neutron-excess nuclides, which show peaks at low bombarding energies, followed by slow decreases as the bombarding energy increases beyond a few hun-

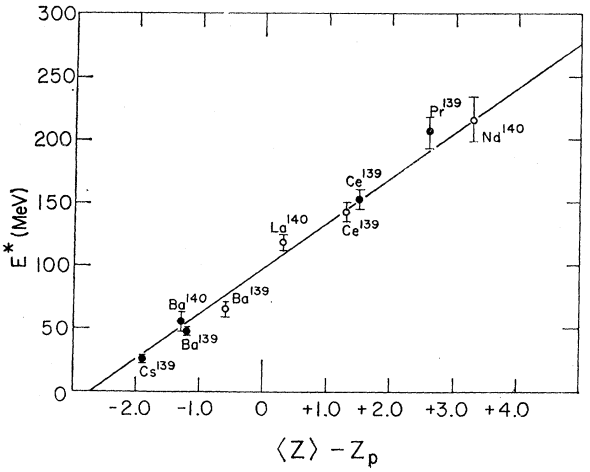

FIG. 11. Isobaric dependence of the cascade deposition energy E^* on the displacement of the average fission-product charge from the most probable charge for mass chains 139 and 140. ○, independently formed nuclides; ●, cumulatively formed nuclides.

dred MeV.[11,39] Second, the production of all nuclides tends to show a preference for certain values of the cascade deposition energy. This point is supported by an analysis of work cited above[4,6,8,11] and work of Crespo *et al.*[10] for a wide range of $\langle N\rangle/\langle Z\rangle$ ratios of fission products.

A linear relationship between the cascade deposition energy and $\langle Z\rangle - Z_p$, the displacement of the average charge from the most probable charge, is given in Fig. 11 for nuclides of mass numbers 139 and 140. The slope of this line is ~35 MeV per charge unit. Previously, a value of 25 MeV per charge unit was reported by Sugarman *et al.*,[8] and a value of 29 MeV per charge unit was suggested by Panontin and Porile[9] in the symmetric fission-product mass region. It should be noted that both of these values were calculated using a somewhat different form of the range-energy equation. Analysis of these data[8,9] using $R \propto T^{1/2}$ yields values of 28 MeV per charge unit and 32 MeV per charge unit, respectively. It is thus apparent that the slope of excitation energy versus $\langle Z\rangle - Z_p$ for heavy fission products is a few MeV per Z unit greater than that averaged over the entire mass region, or that in the region of symmetric fission. What is perhaps most surprising is that this linearity exists over a range of 5.2 charge units, and for deposition energies varying by a factor of 9, from 25 to 225 MeV.

The slope of the E^*-Z dependence of Fig. 11 is also directly related to the momentum-excitation energy relation derived from the Vegas STEPNO calculation,[26] since E^* is calculated from the experimentally measured number $\eta_{||}$. A different model of the proton-nucleus interaction could yield a significantly different value of the slope of the E^*-Z curve. For example, the collision model of Turkevich, as quoted by Porile and Sugarman,[2] gives E^*/E^*_{CN} equal to $p_{||}/p_{CN}$. This would yield a slope 14% greater than 35 MeV per charge unit, or 40 MeV per charge unit. On the other hand, Alexander *et al.*[4] used the relationship E^*/E^*_{CN} equal to $0.75p_{||}/p_{CN}$, yielding a slope of 32 MeV per Z unit. In all of these approaches, however, there is a linear dependence of the excitation energy deposited in the struck nucleus on $\langle Z\rangle - Z_p$.

3. *Angular Distribution of Fission Products*

The angular distribution of the fission products was taken to be of the form $a+b\cos^2\theta$, where θ is the angle between the beam axis and the flight direction of the fission product. The recoil properties of a fission product are used to calculate the ratio b/a as discussed in Sec. III. This value of b/a is the same as that for the primary fission process if the evaporation of particles in the deexcitation of the primary fission fragment does not, on the average, alter the direction of flight.

The value of b/a for each observed nuclide is plotted in Fig. 8 against the cascade deposition energy leading to that nuclide. As was first observed by Sugarman *et al.*,[8] there is an increase in b/a from about -0.1 to about $+0.2$ as the cascade deposition energy increases from 0 to 250 MeV.

The anisotropy of fission fragments is a consequence of their preferential emission in a plane perpendicular to the direction of the angular momentum vector[40] of the fissioning nucleus. Since the angular momentum vector of a compound nucleus is oriented perpendicular to the beam direction, b/a is positive, i.e., preferential emission occurs along the beam direction. The theoretical results of Bohr,[40] Halpern and Strutinski,[41] and Griffin,[41] have been used to analyze the experimental results for low-energy fission following compound-nucleus formation.

The situation in high-energy fission is considerably more complex. The intranuclear cascades result in the production of excited nuclei whose angular momentum vectors vary considerably in magnitude and direction. Until recently, no calculation had been made of the angular momentum of a nucleus resulting from the cascade process. The Vegas calculation of Chen *et al.*,[26] which has been used in this work for correlating linear momentum and cascade deposition energy, also provides for calculation of the total angular momentum of the cascade nucleus and its projection along the beam axis. The first use of these calculations to explain the fission-product anisotropies observed in high-energy fission[8] was made by Crespo, Cumming, and Poskanzer.[10] They explained the qualitative features of the variation

[39] S. S. Parikh, D. A. Marsden, N. T. Porile, and L. Yaffe, Can. J. Chem. **45**, 1863 (1967).

[40] A. Bohr, in *Proceedings of the International Conference on the Peaceful Uses of Atomic Energy* (United Nations, New York, 1956), Vol. 2, p. 151.

[41] I. Halpern and V. M. Strutinski, in *Proceedings of the Second International Conference on the Peaceful Uses of Atomic Energy* (United Nations, Geneva, 1958), Vol. 13, p. 408; J. J. Griffin, Phys. Rev. **116**, 107 (1959).

in b/a observed by Sugarman *et al.*[8] and this work, that of negative b/a for low deposition energy events and positive b/a for high deposition energy events.

For low deposition energy events, the presence of an excess of angular momentum vectors oriented nearly parallel to the beam results in the emission of fission products preferentially in a plane perpendicular to the beam axis, i.e., negative b/a. In the region of deposition energy around 100 MeV, the angular distribution of the angular momentum vectors is essentially isotropic so that b/a is about zero. Finally, at large deposition energies, the angular momentum vectors are oriented preferentially at angles close to 90° to the beam, resulting in the emission of fission products preferentially along the beam axis, i.e., positive b/a. In the three cases, the magnitude of the angular momentum vector was reasonably independent of angle.

The success of this qualitative approach made it of interest to attempt quantitative calculations to determine the value of b/a, as well as its sign. The calculation made use of the expression derived by Leachman and Sanmann[42] based on the fission anisotropy theory proposed by Bohr.[40] The ratio of the differential cross section per unit solid angle for the production of fission products at 0° to that at 90° in the frame of the fissioning nucleus is given by

$$\frac{\omega(0°)}{\omega(90°)} = \frac{\{\exp(-\mathbf{M}^2/2K_0^2)\}}{\{\exp[(\mathbf{M}^2-\mathbf{I}^2)/4K_0^2]\}\{J_0(i(\mathbf{I}^2-\mathbf{M}^2)/4K_0^2)\}}, \quad (11)$$

where $\mathbf{I}$ is the total angular momentum of the fissioning nucleus; $\mathbf{M}$ is the projection of $\mathbf{I}$ on the beam axis; J_0 is the zeroth-order Bessel function; and K_0^2 is given by $T\mathcal{I}_{\text{eff}}/\hbar^2$, with T the nuclear temperature, and $\mathcal{I}_{\text{eff}}$ the effective moment of inertia of the fissioning nucleus. In the derivation of Eq. (11), it was assumed that the nucleus is in a state of statistical equilibrium at the saddle point.

The calculation was performed for cascade nuclei from the Vegas STEPNO calculation[26] for 380-MeV protons bombarding U^{238}. The angular momentum data were not corrected for the difference in bombarding energies of the calculation and experiment. Three deposition energy regions were considered—20–40 MeV, 120–140 MeV, and 200–220 MeV, corresponding to regions of negative, zero, and positive values of b/a, respectively. The calculated results of 2500 cascades for 380-MeV protons on U^{238} contained about 125 events in each excitation energy region.

The cascade deposition energy used to calculate the nuclear temperature in the expression for K_0^2 was corrected for the effect of prefission neutron evaporation and the height of the fission barrier. Calculation of the excitation energy of the fissioning nucleus (discussed in Sec. V A) showed that on the average the cascade deposition energy was reduced by about 10% by particle evaporation prior to fission. The cascade deposition energy was then further reduced by 5.5 MeV, corresponding to the height of the fission barrier[43] in the region of nuclides neighboring on U^{235}. The corrected excitation energy was used to calculate the nuclear temperature by the relation $T=(E/a)^{1/2}$, where a is A of the fissioning nucleus divided by 10.5.

TABLE VI. Calculated and experimental angular anisotropies of fission products.

	$\mathcal{I}_{\text{eff}}$	E^* (MeV) 20–40	120–140	200–220
Expt		−0.10	+0.02	+0.18
Calc	$\mathcal{I}_{\text{sph}}/0.7$	−0.07	+0.07	+0.16
	$\mathcal{I}_{\text{sph}}/0.8$	−0.08	+0.08	+0.18
	$\mathcal{I}_{\text{sph}}/0.9$	−0.09	+0.09	+0.20
	$\mathcal{I}_{\text{sph}}/1.0$	−0.10	+0.10	+0.22

The value of $\mathcal{I}_{\text{eff}}$ used in the calculation was allowed to vary from that of a rotating sphere $\mathcal{I}_{\text{sph}}$ with radius r taken to be $1.4\times10^{-13}A^{1/3}$ cm to $1.43\mathcal{I}_{\text{sph}}$.[44] Results discussed below show that the calculated values of the anisotropy do not change appreciably over the range of values of this parameter.

For each cascade nucleus, with its associated values of $\mathbf{I}$, $\mathbf{M}$, and cascade deposition energy, the production ratio at 0° and 90° was calculated, and related to b/a by the equation $b/a=[\omega(0°)/\omega(90°)]-1$. Since the normalization factor for the distribution $a+b\cos^2\theta$ is $a+\frac{1}{3}b$, for each cascade, $\omega(0°)=(1+b/a)/(1+\frac{1}{3}b/a)$ and $\omega(90°)=1/(1+\frac{1}{3}b/a)$.

This calculation was carried out for each cascade in a given deposition energy bin, and the sums of $\omega(0°)$ and $\omega(90°)$ were calculated. These yield an average value of b/a for all cascade events in a given region of E^*.

The results of the calculation are compared with experimental values in Table VI for four assumed values of the effective moment of inertia.

A least-squares fit of the results for each of the four $\mathcal{I}_{\text{eff}}$ values to the experimental results shows that the best fit is the one for which $\mathcal{I}_{\text{eff}}$ equals $\mathcal{I}_{\text{sph}}/0.8$, in essential agreement with previous work.[44] The calculated results are, however, relatively insensitive to this parameter.

The fit to the experimental values is perhaps somewhat better than might have been expected. The Vegas

[42] R. B. Leachman and E. E. Sanmann, Ann. Phys. (N.Y.) 18, 274 (1962).

[43] W. D. Myers and W. J. Swiatecki, University of California Radiation Laboratory Report No. UCRL-11980, 1965 (unpublished).

[44] J. E. Gindler and J. R. Huizenga, in *Nuclear Chemistry*, edited by L. Yaffe (Academic Press Inc., New York, 1968).

TABLE VII. Average fissioning nucleus leading to observed products.

Product	Z_f	A_f	E_f^*
$Ba^{(133+135)m}(I)$	92.2	234.0	117.2
$Pr^{138}(I)$	91.6	233.5	205.4
$Nd^{138}(I)$	92.2	234.4	225.4
$Cs^{139}(C)$	91.7	235.3	18.2
$Ba^{139}(I)$	91.8	235.0	66.7
$Ce^{139}(I)$	92.6	235.1	119.4
$Pr^{139}(C)$	92.1	234.1	191.0
$Ba^{140}(C)$	92.2	235.2	41.3
$La^{140}(I)$	91.6	235.6	112.9
$Nd^{140}(I)$	92.6	234.6	204.7
$Ce^{141}(C)$	92.2	234.8	87.8
$Pr^{142}(I)$	92.5	235.4	117.4
$Ce^{143}(C)$	92.4	236.1	40.4
$Pr^{143}(I)$	92.6	235.5	104.2
$Ce^{144}(C)$	92.3	234.8	25.8
$Pr^{145}(C)$	91.5	235.9	10.7
$Nd^{147}(C)$	92.5	234.4	14.9

calculation[26] which provides the data on **I** and **M** was performed in a strictly classical manner, in that the angular momentum is not quantized, and the intrinsic spin of the cascade nucleus is not considered. The assumption has also been made, in using the **I** and **M** for the cascade nucleus in the calculation, that prefission particle evaporation does not affect the angular momentum or its projection along the beam axis in any substantial way. Previous to this calculation, the Bohr fission anisotropy theory,[40] as extended by Halpern and Strutinski,[41] Griffin,[41] and Leachman and Sanmann,[42] had not been tested in fission induced by particles of bombarding energy greater than ~40 MeV. It is reasonable to assume, however, that the statistical theory responsible for the assumptions that the **K** distribution is Gaussian, and that $K_0^2=T\mathcal{I}_{\text{eff}}/\hbar^2$, is at least as good for high-energy fission as for 40-MeV fission. It is also reasonable to assume that the values of **I** and **M** remain constant as the fissioning nucleus deforms to the saddle configuration and on to scission since they are "good" quantum numbers.

It has been suggested[45,46] that prefission particle evaporation may take place to a large extent in the case of high-cascade-deposition-energy events. Since K_0 is dependent upon the nuclear temperature, it was considered of interest to perform the calculation of b/a for cascade nuclei of high deposition energy after reduction of their excitation energy by an amount sufficient to evaporate about eight, rather than about two, neutrons. Using the formalism discussed above, and the assumption that $\mathcal{I}_{\text{eff}}=\mathcal{I}_{\text{sph}}/0.8$, the calculated value of b/a, after evaporation of eight neutrons, is 0.23 rather than 0.18. This small overemphasis of the anisotropy in the fission of less-excited nuclei may lend support to the assumption used in this work and discussed in Sec. V A, that even in the case of high-deposition-energy events, fission occurs relatively early in the deexcitation process. Unfortunately, the insensitivity of b/a to the nuclear temperature precludes using this calculation to make definitive statements regarding the length of the prefission evaporation chain. At the very least, however, it may be stated that fission from high-deposition-energy events does not appear to occur at the end of the particle evaporation chain. In this case, the calculated value of b/a is 0.42, considerably greater than that observed experimentally. No correction was made in this case for the effect of evaporation on the anisotropy factor.

V. DISCUSSION OF PROPERTIES OF PRIMARY FISSION FRAGMENTS

A. Calculation of Properties of Primary Fission Fragments

1. Average Fissioning Nucleus Leading to an Observed Fission Product

The *average* fissioning nucleus responsible for the formation of the observed fission products was calculated from the output of the Vegas STEPNO calculation[26] by the following procedure. For each measured fission product, ten cascade nuclei having values of the excitation energy deposited and parallel momentum transferred closely corresponding to values measured in the recoil experiments were chosen randomly. Each of these was used as the initial nucleus in 20 evaporation calculations in which fission was a competing process. The fissionability parameter used was a function of Z and A of the nucleus under consideration, but was *independent* of the excitation energy.[47] The ratio of the probability for fission to the probability for neutron evaporation, Γ_f/Γ_n, is given in Eq. (12), which was derived from the fissionability data collected by Gindler and Huizenga.[44]

$$\Gamma_f/\Gamma_n=\exp[0.343(C_Z-\mathrm{A})], \qquad (12)$$

where $C_{93}=238.88$, $C_{92}=234.07$, $C_{91}=229.92$, $C_{90}=224.80$, and $C_{89}=220.96$.

At each step along the evaporation chain, fission competition was included. If fission did not occur, the product nucleus resulting from further evaporation was then "tested" for fission. In this manner, the average values of Z_f, A_f, and E^*_f were calculated for cascade

[45] Y. LeBeyec, M. Lefort, and J. Peter, Nucl. Phys. **88**, 215 (1966).
[46] Z. Fraenkel (private communication).
[47] M. Lindner and A. Turkevich, Phys. Rev. **119**, 1632 (1960).

nuclei having the appropriate average values of linear momentum transfer and cascade deposition energy for each observed fission product. These values are listed in Table VII.

It may be noted that there is no striking dependence of the calculated values of Z_f and A_f on the average excitation energy at fission. This is a result of the excitation-energy–independent fissionability parameter used in these calculations. Although there is a significant difference in the average values of Z and A of the cascade nucleus for low (~50 MeV) and high (~200 MeV) deposition energy events, this difference essentially disappears in the calculation of the average fissioning nucleus. An average fissioning nucleus with $\langle Z_f \rangle$ of 92.2 and $\langle A_f \rangle$ of 234.9 was used in the calculation of the properties of the primary fragments. These properties are not altered appreciably if somewhat different values of $\langle Z_f \rangle$ and $\langle A_f \rangle$ are used.

2. *Calculation of Properties of Primary Fission Fragments*

The primary fission fragments leading to the observed fission products were calculated by the procedure discussed below, which is based on the formalism of Sugarman *et al.*[8] In all cases, the primed quantities refer to the primary fragments, the unprimed quantities to the observed fission products, and those subscripted "f" to the fissioning nucleus. The following assumptions were made:

(a) The kinetic energy of the fission fragment leading to an observed product is related to that of the observed product by the relation

$$T(Z', A') = T(Z, A) \times A'/A. \tag{13}$$

The assumption inherent in this equation is that the average velocity of the fission fragment is unchanged by successive particle evaporations, consistent with isotropic evaporation of nucleons in the moving frame. The effect of evaporation is a reduction in the kinetic energy of the fragment proportional to the reduction in its mass.

(b) The total kinetic energy of the two fission fragments in the fissioning system, T^{tot}, is divided between them in accord with the conservation of momentum, so that

$$T^{\text{tot}} = T(Z', A')/(1 - A'/A_f). \tag{14}$$

(c) The total excitation energy of the two primary fragments, $E^{*\text{tot}}$, is given by the excitation energy of the fissioning nucleus, corrected for the mass-energy release in the fission process leading to particular fragments, the total kinetic energy calculated from Eq. (14), and the energy attributed to prompt γ-ray emission,[8] 7.5 MeV.

$$E^{*\text{tot}} = E^*_f + M(Z_f, A_f) - [M(Z', A') + M(Z_f - Z', A_f - A')] - T^{\text{tot}} - 7.5 \text{ MeV}, \tag{15}$$

where $M(Z, A)$ is the mass in MeV of the nuclide Z^A. The masses used were those calculated by Myers and Swiatecki.[43]

(d) The total excitation energy is divided between the two fragments such that the excitation energy of a fragment is proportional to its mass.

$$E^*(Z', A') = E^{*\text{tot}} \times A'/A_f. \tag{16}$$

This assumption requires that there is thermodynamic equilibrium in the fissioning nucleus at the time of scission. Harp *et al.*[48] have shown that even in the case of very large excitation energy (~1000 MeV), in times very short ($<10^{-20}$ sec) compared to that required for fission, the excitation energy is partitioned in close accord with thermodynamic equilibrium.

This assumption is invalid in the case of spontaneous fission[49] and thermal neutron fission of U.[50] Measurement of the number of neutrons associated with production of nuclides of a given mass shows a sharp discontinuity with increasing mass in the symmetric fission region in both of these cases.

Unpublished work of Fraenkel *et al.*[46] on 150-MeV proton fission of U shows that a plot of the average number of neutrons associated with the production of a given mass versus A is continuous over the fission-product mass region; it is not linear, however, as would be expected from the assumption used above. The validity of this assumption will be considered further in Sec. V B in which the excitation energy of the primary fragments is discussed.

(e) The primary fragment with excitation energy $E^*(Z', A')$ is deexcited by particle evaporation in accord with the Porile evaporation calculations,[51] based on work by Dostrovsky *et al.*[52] The level-density parameter a was taken to be $A/10.5$.

3. *Properties of Primary Fragments*

a. Primary fragments leading to independent fission products. The calculation was performed by first selecting all conceivable fragments which could lead to an observed independent fission product. The quantities, $E^*(Z', A')$, $T(Z', A')$, $E^{*\text{tot}}$, T^{tot}, were calculated, as discussed above, and the values of Z', A', and $E^*(Z', A')$ were used as the input data in an evaporation calculation. Twenty to fifty evaporations were carried out on each trial fission fragment; the larger number was used for fragments leading to many products. In all cases, enough evaporations were carried out on the trial fission fragments to produce the observed fission product some ten to twenty times. Those evaporations which yielded the observed fission product were col-

[48] G. D. Harp, J. M. Miller, and B. J. Berne, Phys. Rev. **165**, 1166 (1968).
[49] S. L. Whetstone, Jr., Phys. Rev. **114**, 581 (1959).
[50] J. Terrell, Phys. Rev. **127**, 880 (1962).
[51] N. T. Porile (private communication).
[52] I. Dostrovsky, Z. Fraenkel, and G. Friedlander, Phys. Rev. **116**, 683 (1960).

TABLE VIII. Properties of average primary fragments leading to independent fission products.

Product	Z'	A'	$E^*(Z', A')$ (MeV)	$T(Z', A')$ (MeV)	E^{*tot} (MeV)	T^{tot} (MeV)
$Ba^{(133+135)m}$	56.0	142.6	91.2	58.2	150.2	148.0
Pr^{138}	59.3	151.4	152.4	50.3	236.6	141.5
Nd^{138}	60.8	152.2	173.0	47.4	267.1	134.5
Ba^{139}	56.0	145.1	48.8	63.6	79.1	166.4
Ce^{139}	58.0	148.3	89.8	57.0	142.3	154.4
La^{140}	57.0	149.2	79.6	58.9	125.3	161.5
Nd^{140}	60.2	152.9	147.1	52.1	226.0	149.2
Pr^{142}	59.0	151.4	90.4	53.6	140.2	150.8
Pr^{143}	59.0	151.3	80.3	54.2	124.5	153.0

lected and the quantities discussed above were averaged.

The results of these calculations are given in Table VIII. Column 1 lists the observed product; columns 2 and 3, the average values of Z' and A' for the fission fragment leading to the observed product; columns 4 and 5, the excitation and kinetic energies of these fragments; and the last two columns, the calculated values of the total excitation energy and kinetic energy of the fragment pair produced in the fission process.

b. Primary fragments leading to cumulative fission products. The calculation described above was carried out *independently* for each β-decaying precursor of an observed cumulative fission product. The dependence of E^* on $\langle N\rangle/\langle Z\rangle$, and T on $(\langle N\rangle/\langle Z\rangle)/A$, for the fission products [Fig. (6) and (7)] were used to determine the values of the excitation and kinetic energies which would have been measured had each of the progenitors been determined independently. In all cases, the values chosen for these quantities were then normalized such that the calculated values for a cumulative product were in agreement with those actually measured.

The average calculated values of the recoil parameters of fission fragments leading to the individual progenitors of an observed product were then weighted by the chain yields of the *products* to calculate grand averages for an observed cumulative product.

The results of these calculations are given in Table IX. Column 1 lists the observed product; column 2, the β-decaying progenitors of the product; columns 3 and 4, the average values of Z' and A' for the fission fragment leading to the observed progenitor; columns 5 and 6, the excitation energy and the kinetic energy of these fragments; and the last two columns, the calculated values of the total excitation energy and kinetic energy of the *two* fragments produced in the fission process. The final *row* under each observed cumulative product lists the grand averages for each of the quantities above.

4. *Errors in Calculation of Properties of Primary Fission Fragments*

The primary source of error in the calculation of the properties of individual primary fragments, other than the errors from the assumptions listed in Sec. V A 2, is the averaging of the calculated quantities of the trial fragments with no weighting for the relative yields of the fragments themselves. For the independent fission products, except for Nd^{138}, Pr^{138}, and Nd^{140}, 80–90% of the observed product was shown to arise from no more than two primary fragments. If the trial primary fragments are produced in equal yield, the average calculated primary fragments are correct to 0.1 charge unit and 1 mass unit, and the values of $E^*(Z', A')$, $T(Z', A')$, E^{*tot}, T^{tot} are correct to 2, 0.5, 3.5, and 1.5 MeV, respectively. These errors represent liberal estimates of the relative contribution from each of the two calculated primary fragments accounting for the bulk of the product.

Much more serious are the errors arising in the calculation of the average primary fragment for the three neutron-deficient products mentioned above. The most extreme case Nd^{138}, with a cascade deposition energy of nearly 250 MeV, was found to be one of the final products arising from a total of 16 different primary fragments. None of the fragments contributed more than 20% of the yield of the product, and none deexcited to Nd^{138} in as many as 50% of its evaporations. These fragments ranged over values of Z' from 60 to 62, and A' from 148 to 155. The Z values of the very neutron-deficient products, Nd^{138}, Pr^{138}, and Nd^{140}, are far from the most probable charge of the fission-product charge dispersion curve. It is likely, therefore, that these neutron-deficient products arise from fragments far from the most probable *fragment* charge, where the relative yields of the fragments are changing most rapidly. It is estimated from the spread in values of the various primary fragments, and the uncertainty in the weighting factors used in averaging, that the

TABLE IX. Properties of average primary fragments leading to cumulative fission products.

Product	Progenitor	Z'	A'	$E^*(Z',A')$ (MeV)	$T(Z',A')$ (MeV)	E^{*tot} (MeV)	T^{tot} (MeV)
1. Pr^{139}							
	Pr^{139}	59.2	151.2	130.8	51.7	203.2	145.2
	Nd^{139}	60.4	153.0	176.0	49.0	270.2	141.6
Average		59.4	151.6	148.7	51.2	214.9	144.5
2. Cs^{139}							
	Cs^{139}	55.0	143.6	30.8	62.1	50.4	159.6
	Xe^{139}	54.0	142.0	17.1	64.7	28.2	163.5
	I^{139}	53.0	140.0	8.5	66.9	14.2	165.5
Average		54.7	143.1	26.6	62.9	43.7	160.8
3. Ba^{140}							
	Ba^{140}	56.0	146.8	54.6	58.7	87.3	156.6
	Cs^{140}	55.0	145.2	36.3	61.3	58.7	160.3
	Xe^{140}	54.0	142.0	15.4	63.3	25.4	160.0
Average		55.5	145.8	44.7	60.0	71.8	158.1
4. Ce^{141}							
	Ce^{141}	58.0	150.1	88.3	56.1	138.0	155.4
	La^{141}	57.0	148.5	62.4	58.6	98.7	159.4
	Ba^{141}	56.0	146.7	41.4	61.1	63.3	162.5
	Cs^{141}	55.0	144.2	22.7	63.2	37.1	163.6
	Xe^{141}	54.0	142.0	8.5	65.5	14.1	165.5
Average		56.6	147.5	54.8	59.6	86.7	160.2
5. Ce^{143}							
	Ce^{143}	58.0	149.9	62.4	55.8	97.8	154.1
	La^{143}	57.0	148.1	40.1	58.1	63.6	157.3
	Ba^{143}	56.0	146.8	25.8	60.7	41.3	161.7
	Cs^{143}	55.0	144.5	11.0	62.9	17.9	163.6
Average		56.9	148.1	41.4	58.4	65.3	157.9
6. Ce^{144}							
	Ce^{144}	58.0	149.7	53.4	52.3	83.8	144.1
	La^{144}	57.0	148.9	37.0	54.9	58.4	150.0
	Ba^{144}	56.0	147.0	24.0	57.2	38.3	152.8
	Cs^{144}	55.0	146.0	20.3	57.6	15.8	157.8
Average		57.0	148.6	39.5	54.5	61.3	148.8
7. Pr^{145}							
	Pr^{145}	59.0	152.1	44.3	54.3	69.0	140.4
	Ce^{145}	58.0	148.9	35.2	53.0	55.4	144.8
	La^{145}	57.0	148.1	25.9	55.3	41.1	150.7
	Ba^{145}	56.0	147.0	14.8	58.1	23.6	155.2
Average		57.7	149.2	32.2	54.6	50.7	146.7
8. Nd^{147}							
	Nd^{147}	60.0	152.0	44.4	54.3	69.2	153.9
	Pr^{147}	59.0	150.7	31.2	56.9	48.7	158.8
	Ce^{147}	58.0	149.0	21.3	59.3	33.6	162.2
	La^{147}	57.0	148.0	10.5	61.9	16.6	167.4
	Ba^{147}	56.0	147.0	2.0	64.8	3.2	173.2
Average		58.4	149.7	25.2	58.5	39.5	161.3

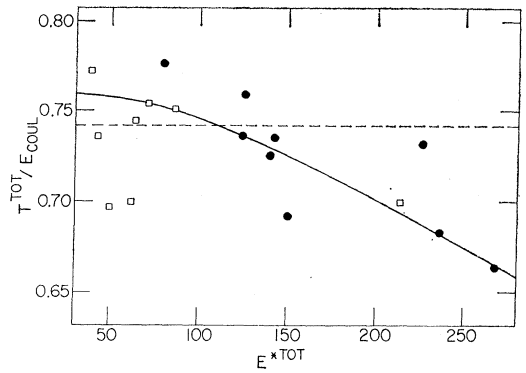

FIG. 12. Variation of the total kinetic energy of a pair of fission fragments divided by their Coulomb energy, T^{tot}/E_{Coul}, with their total excitation energy E^{*tot}. ●, this work, independent nuclides; □, this work, cumulative nuclides; the dashed line is from Crespo *et al.* (Ref. 10).

maximum errors of Z', A', $E^*(Z', A')$, $T(Z', A')$, E^{*tot}, and T^{tot} are 0.5 charge unit, 2.5 mass units, 3, 1, 8, and 4 MeV, respectively, for these three nuclides.

In the case of cumulative fission products, the same assumption of constant yield was made in averaging the primary fragments leading to each progenitor. With the exception of the production of Pr^{139}, no β-decaying precursor of a cumulative fission product was formed from more than three fragments. In all of these cases, one or two fragments accounted for 90% of the total production of the progenitor. The errors in the calculated properties of each progenitor of a cumulative fission product are then similar to those discussed above for independent products. The average primary fragment leading to each of the progenitors of the cumulative products, as well as the average primary fragment for all the cumulative products themselves, (except Pr^{139}) may be considered to have a maximum error in Z', A', $E^*(Z', A')$, $T(Z', A')$, E^{*tot}, and T^{tot} of 0.1 charge unit, 1 mass unit, 2, 0.5, 3, and 1 MeV, respectively. In the case of Pr^{139}, serious errors arise for both independently formed Pr^{139}, and its progenitor Nd^{139}. $Pr^{139}(I)$ arises from six fragments. Nd^{139} arises from ten fragments, no one of which accounts for as much as 20% of the total production of Nd^{139}. It is estimated that for both of these progenitors of $Pr^{139}(C)$, as in the case of the three independently measured neutron-deficient nuclides, the maximum errors for the independently formed species are 0.5 charge unit, 2.5 mass unit, 3, 1, 8, and 4 MeV for Z', A', $E^*(Z', A')$, $T(Z', A')$, E^{*tot}, and T^{tot}, respectively.

There is a second source of error in the primary-fragment calculation for cumulative fission products. In the calculation of the average fragment leading to a cumulative product, the average fragment leading to each β-decaying precursor was weighted by the relative yield of the precursor, as determined by the fission-*product* charge dispersion curve. Insofar as the calculated properties of the average fragment for each precursor are valid, the weighted (by relative yields) grand average for the cumulative product should also be valid. Errors may arise, however, in the determination of these weighting factors. They are, of necessity, taken from a fission-product charge dispersion curve which is not experimentally defined for nuclides far from the most probable charge.

An estimate of the consequences of this source of error may be made for any given nuclide by calculating the effect of neglecting a given progenitor on the average values of the properties of the primary fission fragments. For example, if I^{139} is *not* a significant progenitor of Cs^{139}, these values calculated for Cs^{139} would be in error by about 4% of the *difference* between the corresponding values for I^{139} and the average values for Cs^{139}.

In light of this discussion, the most serious error in the calculation of the primary fragments is expected in the case of $Pr^{139}(C)$. Its progenitor Nd^{139} lies 3.4 charge units from the most probable value for mass chain 139; therefore, the relative weights for the average fragments leading to it and to $Pr^{139}(I)$ are not well known. Second, the products Nd^{139} and Pr^{139} arise from high-deposition-energy events. The calculated average fragment leading to each of them may be in serious error because of the multiplicity of calculated primary fragments. The over-all error associated with the calculated values for the average fragment leading to $Pr^{139}(C)$ are 0.7 charge units, 3.0 mass units, 5, 1.5, 11, and 6 MeV, in Z', A', $E^*(Z', A')$, $T(Z', A')$, E^{*tot}, and T^{tot}, respectively.

B. Results of Calculation of Properties of Primary Fragments Leading to Observed Fission Products

1. *Relationship of Average Total Kinetic Energy and Excitation Energy of Primary Fragments*

The average total kinetic energy and excitation energy, T^{tot} and E^{*tot}, of the average primary-fragment pair leading to each observed fission product are related to the nuclear configuration at scission. The *ratio* of the average total kinetic energy for a given pair of primary fragments, T^{tot}, to the calculated Coulombic energy at scission, E_{Coul}, on the assumption that the two fragments are spheres in contact, is plotted against the total excitation energy of the two fragments (see Tables VIII and IX) in Fig. 12. In this calculation, the nuclear radius parameter was taken to be 1.40 F. This ratio T^{tot}/E_{Coul} decreases with increasing E^{*tot} by about 12% from the lowest value of E^{*tot}, ~40 MeV, to the highest ~260 MeV. The decrease is somewhat less, about 11% instead of 12%, if a dispersion in **V** (see Sec. IV B 1) is included in the calculation of T^{tot}/E_{Coul}. A least-squares fit of the data to a straight line (not shown) gives $T^{tot}/E_{Coul}=(0.762\pm0.013)-(2.76\pm0.88\times10^{-4})E^{*tot}$. The slope is negative, lying

3.1 standard deviations from a horizontal line. A hyperbolic curve gives a slightly better fit, $T^{\text{tot}}/E_{\text{Coul}}=1/\{(1.31\pm0.20)+(5.40\pm1.40\times10^{-4})E^{*\text{tot}}\}$. The errors in each case are calculated from the scatter of the data about the "best-fit" line. No attempt was made to evaluate the errors in the data, or to weight the data in the computation of the best-fit curve, since no quantitative estimate can be made of the errors from the assumptions used to calculate these points. The precision error in the kinetic energy of the fission products is about 1.5% (Table V), corresponding to about 0.01 in the ratio $T^{\text{tot}}/E_{\text{Coul}}$.

The decrease of $T^{\text{tot}}/E_{\text{Coul}}$ with increasing $E^{*\text{tot}}$ indicates that the distance between the charge centers of the primary fragments (which are taken to be spherical) increases with increasing $E^{*\text{tot}}$, from 17.5 to 19.6 F. The negative dependence of the scission distance on $E^{*\text{tot}}$ is not significantly affected by either the assumption that the fissionability parameter is independent of excitation energy, or that the total excitation energy available to the fragments is divided in proportion to the fragment masses. A different fissioning nucleus, in particular a fissioning nucleus whose mass is a function of the initial excitation energy, would of course produce a change in the calculated properties of the primary fragments. If the assumption is made that high-deposition-energy processes lead to fissioning nuclei which are most neutron-deficient,[45,46] one would expect correspondingly fewer neutron-excess primary fragments for these events. It may be shown that if the fissioning nucleus is U^{234} for neutron-excess products from low-deposition-energy events, and U^{228} for neutron-deficient products from high-deposition-energy events, the slope of Fig. 12 would become more negative, largely due to a substantial reduction in the calculated value of $E^{*\text{tot}}$. The value of $T^{\text{tot}}/E_{\text{Coul}}$ is reduced $\sim$2% in the case of the most neutron-deficient products, while $E^{*\text{tot}}$ is reduced roughly by the excitation energy required to evaporate six more neutrons prior to fission. The over-all effect is to move the high-deposition-energy events toward significantly lower values of $E^{*\text{tot}}$, making the observed slope more negative.

It is also necessary to consider the effect of the assumption relating the excitation of a given primary fragment to the total excitation energy of the fissioning nucleus. If the heavy fragment receives less excitation energy than that calculated from its proportionality to mass [Eq. (16)], as indicated by the results of Fraenkel[46] on 150-MeV fission of Bi and U, the slope of Fig. 12 again becomes more negative. The primary fragment, produced with a smaller excitation energy, would have a smaller mass, and, from Eqs. (13) and (14), a lower value of $T^{\text{tot}}/E_{\text{Coul}}$. There would be an increase in $E^{*\text{tot}}$ from the mass-energy release because the mass split is less asymmetric. This increase in $E^{*\text{tot}}$ is small compared to the decrease in $T^{\text{tot}}/E_{\text{Coul}}$. The over-all effect is still a more negative slope of the curve of Fig. 12.

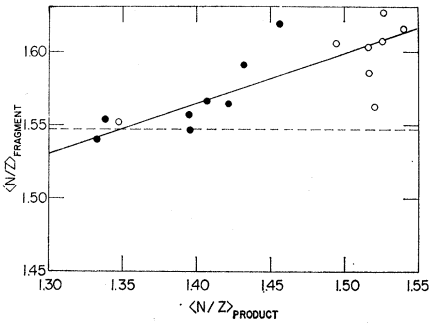

FIG. 13. Relationship between the average neutron-to-proton ratio of the primary fragments and the average neutron-to-proton ratio of the products to which they deexcite. ●, independent nuclides; ○, cumulative nuclides. The dashed line is from Crespo *et al.* (Ref. 10).

In order to ensure that the negative slope of Fig. 12 is not a consequence of the momentum-excitation energy relation used (Fig. 4), calculations were also performed using two other dependences, $E^*/E^*_{\text{CN}}=0.70p_{||}/p_{\text{CN}}$ and $E^*/E^*_{\text{CN}}=1.0p_{||}/p_{\text{CN}}$. In the former case, the slope of the curve becomes more negative; in the latter case, the slope becomes about 20% less negative.

The range-energy formulation[8] $R=CT^{N/2}$ leads to slightly larger absolute values of the kinetic energy, but to nearly the identical dependence of the kinetic energy on N/Z (see Sec. IV B 1). Equations (13) and (14) may be combined to show that the calculated values of T^{tot} and $T^{\text{tot}}/E_{\text{Coul}}$ are directly proportional to T, with minor corrections arising from a small variation in A'. Thus, while the form of the range-energy equation affects the absolute value of $T^{\text{tot}}/E_{\text{Coul}}$, its dependence on $E^{*\text{tot}}$ is essentially unaffected.

2. *Relationship of Neutron-to-Proton Ratio of Average Primary Fragment Leading to an Observed Product to that of the Fission Product Itself*

The neutron-to-proton ratio of each average primary fragment, calculated from data in Tables VIII and IX, may be compared with that of its associated fission product (Table V). The relationship between these quantities is shown in Fig. 13. It is evident that the charge dispersion of the average primary fragments is less than that observed in the fission products. This result suggests that the increase in the width of the charge dispersion curve at a given mass from 440-MeV proton fission (FWHM $\sim$3.2 charge units), from that observed in thermal neutron fission (FWHM $\sim$2.2 charge units), may arise principally from increased neutron evaporation of the primary fragments leading to the observed fission products. The primary division of charge between the two fragments does not appear to be very dependent upon the energy of the incident particle. The average fragment leading to a neutron-excess product with mass 140 is itself neutron-excess

TABLE X. Properties of average primary fragments leading to fission products in the complementary and symmetric mass regions.

Product	Z'	A'	$E^*(Z', A')$ (MeV)	$T(Z', A')$ (MeV)	E^{*tot} (MeV)	T^{tot} (MeV)
Sr^{89}	36.8	93.7	61.5	85.8	151.6	144.0
Sr^{91}	37.2	97.0	60.2	85.1	144.2	146.1
Mo^{99}	40.9	104.0	68.5	80.1	152.4	145.7
Ru^{103}	42.4	107.4	72.5	78.3	155.0	147.3
Pd^{103}	46.8	111.4	105.6	83.2	222.5	158.6
Ru^{106}	43.3	112.9	75.2	76.1	154.4	147.8
Pd^{109}	44.8	115.0	82.1	74.8	165.2	148.7
Ag^{111}	45.6	117.3	83.9	74.0	165.2	150.2
In^{111}	49.8	121.4	119.7	68.6	253.2	141.8

relative to the fissioning nucleus. The neutron-deficient products, on the other hand, arise from primary fragments which are neutron-excess, but less so than the fissioning nucleus.

These results are essentially unaffected by the substitution of 0.7 or 1.0 in the slope of dependence of the excitation energy on momentum transfer [Eq. (6)].

The mean velocity of a primary fragment leading to a product may also be calculated by the method of Crespo *et al.*[10] from the theory of Nix and Swiatecki.[53] In this method, the primary fragment is assumed to have the same charge-to-mass ratio as the fissioning nucleus, taken to be $U^{234.4}$. The primary fragment of charge Z' and mass A' yields a fission product (Z, A) by evaporation of neutrons *only* (Z equals Z') with no change in the mean velocity. The kinetic energy of the primary fragment, and that of its associated fission product, are thus related by the ratio of the masses A' and A. The kinetic energy of each of the fission products studied in this work was calculated by this procedure and the results show the same trend as that of Fig. 6. The calculated values, though, are uniformly about 1.7 MeV higher than the corresponding values on the curve of Fig. 6. There is no *dependence* of the neutron-to-proton ratio of the primary fragment on that of the product, since $\langle N/Z \rangle$ for the fragment is assumed to be that of $U^{234.4}$, i.e., 1.55 (see Fig. 13). There is also no dependence in the Nix-Swiatecki theory, other than the Coulombic dependence, of the total kinetic energy of the fragment pair on $\langle N/Z \rangle$ or E^{*tot} for the product. The ratio T^{tot}/E_{Coul} is 0.742 (see Fig. 12). The determination of the primary fragments by the assumption of unchanged charge distribution results in a much stronger dependence of the excitation energy of the fragment on $\langle N/Z \rangle$ of the product than that calculated in this work.

[53] J. R. Nix and W. J. Swiatecki, Nucl. Phys. **71**, 1 (1965).

3. *Calculation of Properties of Average Primary Fragments Leading to Fission Products in Lower Mass Regions*

The properties of the primary fission fragments leading to products in the region of mass roughly complementary[8] to that of $A \sim 140$ and in the symmetric region[9] were obtained from data of Sugarman *et al.*[8] and Panontin and Porile.[9] The results of this analysis are listed in Table X, and are plotted in Figs. 14 and 15, where the dotted lines are the same as the solid lines shown previously in Figs. 12 and 13. The same dependence of the total kinetic energy on the excitation energy of the average primary fission fragments seen in Fig. 12 is clearly present.

While data in the mass region $A = 72$ from Sugarman *et al.*[8] were not included in this analysis, the trends observed in the kinetic and excitation energies of the fission products, Ga^{72}, Zn^{72}, and Ga^{73}, the values of T^{tot} and E^{*tot} for the fission fragments corresponding to these products, and the scission distance derived from these values, are all consistent with the trends observed in Figs. 14 and 15.

Panontin and Porile[9] used a different range-energy equation, and slightly different assumptions in calculating the properties of the primary fragments. The present analysis slightly changes the values of T^{tot}/E_{Coul} and E^{*tot} from those reported by Panontin and Porile, but the pattern of the results is essentially unchanged. The more limited data of Panontin and Porile do not by themselves establish the trend observed in this work.

The difference in the magnitude of T^{tot}/E_{Coul} at a given E^{*tot} between the heavy and symmetric mass eegions may be attributed to the apparent kinetic enrrgy deficit of 7–10 MeV observed in symmetric fission, discussed by Sugarman *et al.*,[8] although no such decrease is expected in the product mass region from

85–100.[8] These lower kinetic energy values may be the result of the fact that nearly all of the data in this mass region are those of cumulative fission products where the greatest uncertainty in averaging the properties of the primary fragments is present. Another source of error is the set of charge dispersion parameters used for cumulative products. There may be an error in the constant value of N/Z_p of 1.420 used for all masses in this region,[9] or in FWHM of the charge dispersion curve, taken to be 2.9 charge units.[9]

The calculated values of $\langle N/Z\rangle_{\text{fragment}}$ are plotted against $\langle N/Z\rangle_{\text{product}}$ for the lighter fission products as well as those of mass about 140 in Fig. 15. The relatively small spread in the average $\langle N/Z\rangle_{\text{product}}$ values precludes making a detailed comparison of the results for the high and low mass region. The line drawn represents the data in the light region better than that (dotted line) previously drawn through the data in the heavy mass region alone (Fig. 15).

There is an apparent inconsistency in the fact that the trends in the two mass regions are similar. In the heavy-mass region, the neutron-deficient high-deposition-energy products are shown to arise from primary fragments which are neutron-deficient relative to the fissioning nucleus. The complementary fragments, neutron excessive relative to the fissioning nucleus, might, incorrectly, then be expected to lead to the high-deposition-energy neutron-deficient products in the light-mass region. Experimentally, however, this is not the case, as shown by Fig. 15. Neutron-deficient products in the light-mass region also arise, on the average, from fragments neutron-deficient relative to the fissioning nucleus.

The explanation of this apparent inconsistency lies in what may be called the "inverse averaging problem." The properties of an observed product are used to calculate the properties of its average primary fragment. These calculated properties of the average primary fragment leading to a given fission product, however, are not necessarily the average properties of that fragment—those obtained by averaging over all fission events leading to the primary fragment. Second, the observed product is not, in general, the average product arising from a given primary fragment. In some cases, of which Nd^{138} is an example, the observed product is not even the average product arising from those fissions in which the given primary fragment *has the average calculated properties.*

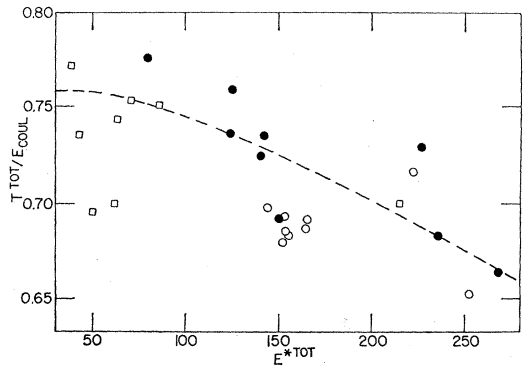

FIG. 14. Variation of the total kinetic energy of a pair of fission fragments divided by their Coulomb energy $T^{\text{tot}}/E_{\text{Coul}}$, with their total excitation energy $E^{*\text{tot}}$. ●, this work, independent nuclides; □, this work, cumulative nuclides; ○, work of Sugarman *et al.* (Ref. 44) and Panontin and Porile (Ref. 39), reanalyzed by the procedure of this work.

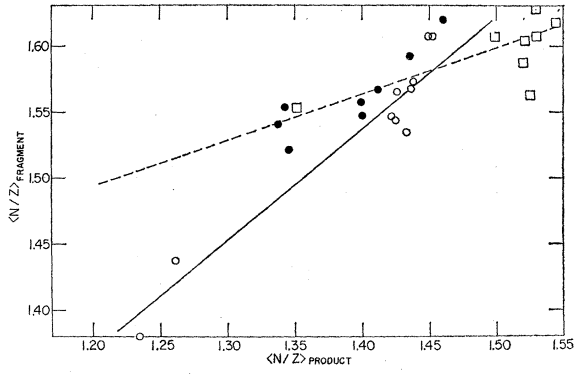

FIG. 15. Relation between the average neutron-to-proton ratio of primary fragments and the average neutron-to-proton ratio of the products to which they deexcite. ●, this work, independent nuclides; □, this work, cumulative nuclides; ○, work of Sugarman *et al.* (Ref. 44) and Panontin and Porile (Ref. 39), reanalyzed by the procedure of this work.

C. Explanation of Properties of Fission Products

1. Kinetic Energy of Fission Products

The kinetic energy of the most neutron-deficient fission product is some 30% lower than that of the most neutron-excess fission product (see Fig. 10). Three effects are responsible for the reduction in kinetic energy with decreasing neutron excess; deformation of the fissioning nucleus, particle evaporation from the primary fragments, and the mass effect on the division of the total kinetic energy between the two fragments.

The first effect amounts to increased excitation energy at the scission point and is thus similar to the case of thermal neutron fission. Evidence which was discussed in Sec. V B shows an increase in the deformation of the fissioning nucleus sufficient to reduce the total kinetic energy of the two fragments by about 10% between the lowest- and highest-deposition-energy fission products.

Second, a large source of excitation energy other than deformation is present in high-energy fission. The initial cascade may deposit several hundred MeV in the fissioning nucleus. Much of this excitation energy eventually is present in the primary fragments resulting in long evaporation chains to the observed fission product. Since the kinetic energy is reduced in proportion to the reduction in mass, as much as 8–10% more

of the primary-fragment kinetic energy may be lost in the evaporation to neutron-deficient products than to neutron-excess products.

Finally, the conservation of momentum determines the division of the total kinetic energy between the two fragments. In particular, a heavier primary fragment receives a lower fraction of the total kinetic energy. As discussed above, the high-deposition-energy products have long particle-evaporation chains. This implies significantly heavier primary fragments being produced with correspondingly lower kinetic energy. In the mass region of interest in this work, the heavier fragments leading to neutron-deficient fission products receive about a 10% smaller share of the total kinetic energy than do the lighter fragments leading to neutron-excess products of the same mass.

Thus, three effects combine in roughly equal amounts to produce the 30% decrease in the kinetic energy of neutron-deficient relative to neutron-excess products. This is in marked contrast to the case of thermal neutron fission where a very nearly equivalent reduction of the kinetic energy, about 6–7% per charge unit,[37] is caused apparently solely by a deformation effect.[38]

The 30% decrease in the kinetic energy of neutron-deficient relative to neutron-excess fission products is also predicted by Crespo *et al.*,[10] using the Nix and Swiatecki[53] theory (see Sec. V B). In this case, the assumption of unchanged charge distribution in the primary fragments increases the magnitude of the second and third effects above in order to compensate for the assumed absence of the first effect. The relatively short evaporation chains to the neutron-excess products calculated in this work become substantially shorter, while the longer evaporation chains to neutron-deficient products become substantially longer.

2. *Cascade Deposition Energy for Formation of Fission Products*

The cascade deposition energy leading to isobaric fission products increases linearly with increasing charge by about 35 MeV per charge unit (see Fig. 11). This difference in deposition energy arises from differences in the following three quantities: the mass-energy release in the production of the primary fragments, the total kinetic energy of the two fragments, and post-scission particle evaporation.

Results of the primary-fragment calculation reported in Tables VIII and IX show that isobaric products which differ by one charge unit arise, in general, from primary fragments differing by one charge and two mass units. The three energy values above change as follows for the fragment or fission fragment pair leading to the more neutron-deficient product. First, the mass-energy release is reduced by ~5 MeV.[43] In this mass region, the addition of a proton to the heavy fragment reduces the mass-energy release by ~1.5 MeV, a neutron by ~3.5 MeV. Second, the total kinetic energy associated with the fragments is reduced by about 2 MeV. This reduction is a product of increased deformation at the higher excitation energy, discussed in Sec. V B. These two effects reduce from 35 MeV to about 32 MeV the increase in excitation energy available to the fragment pair leading to the more neutron-deficient isobaric product.

Third, this 32 MeV is divided between the two fragments in direct proportion to their masses. A fragment of mass 150 will receive about 20.5 MeV—just enough to evaporate two neutrons, and yield a product with one more charge than its more neutron excess isobaric partner.

VI. SUMMARY AND CONCLUSIONS

The charge dispersion curve for fission products of mass 139, formed in the 440-MeV fission of U, was measured and found to have a FWHM of 3.2 charge units. This value is in agreement with that reported by Folger *et al.*,[28] Panontin and Porile,[9] Hagebø,[12] and Sugarman *et al.*[8] The discrepancy between this value and that of Friedlander *et al.*,[11] 5.2 charge units, was partly resolved by use of a mass-dependent most-probable neutron-to-proton ratio for the fission products.

The recoil properties of 17 nuclides were determined and those of three nuclides were calculated by use of the measured charge dispersion curve. The range of a fission product, calculated from its recoil properties, was used to calculate the kinetic energy by a linear range-velocity relation.

The velocity imparted to the cascade nucleus, calculated from the ratio of this velocity to that of the fission fragment in the moving frame, was related to the excitation energy deposited in the cascade nucleus. Finally, the difference in the measured "apparent" ranges in forward-backward and perpendicular experiments was related to the angular anisotropy of fission products. The principal results of the recoil properties of *isobaric* fission products may be summarized:

(1) The kinetic energy of fission products decreases linearly with increasing charge by about 2% per charge unit.

(2) The cascade deposition energy increases linearly with increasing charge approximately 35 MeV per charge unit.

(3) The anisotropy of the angular distribution changes with increasing cascade deposition energy from preferential emission perpendicular to the beam direction at low deposition energy to preferential emission along the beam direction at high deposition energy. This change in the anisotropy was accounted for by use of the angular momentum data of the cascade nucleus and the theoretical approach applied previously to fission induced by protons of less than 40 MeV.

The recoil properties of the fission products were related to those of the primary fission fragments from which the fission products arise by particle evaporation. Results of this calculation were used to explain the observations on kinetic energy and deposition energy mentioned above. The decrease in kinetic energy for a more neutron-deficient fission product was found to arise from three sources, contributing nearly equally. First, high deposition energies were found to cause increased deformation in the fissioning nucleus with consequent reduction of the Coulombic repulsion between the primary fragments at scission. Second, a neutron-deficient product arises from a heavier, more highly excited, primary fragment which is deexcited by a longer evaporation chain. The heavier fragment has a smaller fraction of the total kinetic energy because of conservation of momentum. Finally, the longer evaporation chain leads to a greater loss of mass, which corresponds to a greater reduction in the kinetic energy of the final fission product.

The increase in excitation energy of 35 MeV per charge unit for isobars was found to arise from one additional proton and one additional neutron in the primary fission fragment. The extra 35 MeV was used up primarily in the increased excitation energy of the primary fission fragment needed to evaporate these two additional nucleons.

The calculated properties of the primary fission fragments show an effect of excitation energy on the scission shape, which affects the kinetic energy of the fission products. This effect, not previously observed in high-energy fission is supported by data on fission products in other mass regions. The charge dispersion of the primary fission fragments is significantly narrower than that of the fission products; the broadening of the charge dispersion is a consequence of post-fission particle evaporation.

Note added in proof. The manuscript of a paper *Recoil Properties of Antimony Isotopes Produced by the Reaction of 570 MeV and 18.2 GeV Protons with Uranium* by Hagebø and Ravn arrived after this paper was submitted for publication. In this paper, Hagebø and Ravn conclude that at 570 MeV "the average total kinetic energy of the primary fragments is smaller and thus the average separation distance of their charge centers at scission larger for the lightest antimony isotopes than for the heaviest, the difference being about 10%." This conclusion, arrived at using a simplified means of calculation of the properties of the primary fission fragments, lends support to the conclusion of this work that the total kinetic energy release is dependent upon the excitation energy of the fissioning nucleus.

ACKNOWLEDGMENTS

The authors wish to thank Dr. K. Chen and Dr. G. Friedlander of Brookhaven National Laboratory for carrying out and making available the results of intranuclear cascade calculations upon which much of the analyses of this work is based. Appreciation is expressed to Dr. E. P. Steinberg and Dr. L. E. Glendenin of Argonne National Laboratory for use of their Li-drifted Ge detectors. K. Sowinski and T. Economou of the Enrico Fermi Institute aided in the writing of the computer programs used in this work. Finally, the authors are pleased to acknowledge many fruitful discussions with Dr. G. Friedlander, Dr. J. B. Cumming, Dr. J. A. Panontin, Professor L. Yaffe, and Dr. L. Remsberg.

APPENDIX A: CHEMICAL AND COUNTING PROCEDURES; RECOIL EXPERIMENTS

1. Cesium

The recoil properties of 9.5-min Cs^{139} were determined indirectly by analysis of the Ba^{139} activity grown from purified Cs.

From each solution of target and catchers, a mixed hydroxide–carbonate of barium and strontium was precipitated in the presence of Cs carrier by addition of $12M$ NaOH and $2M$ Na_2CO_3. After digestion of the precipitate for 1 min, the solution was filtered through a double layer of hardened biological filter paper which allowed negligible flow under gravity. Vacuum was then applied in parallel to the three Büchner funnels so that the solutions were filtered and the precipitates washed in a few seconds. This time, usually about 15 min from the end of irradiation, is the time zero for growth of 85-min Ba^{139}.

There was no quantitative measure of the recovery of Cs in the filtration; however, experiments using Cs^{137} tracer showed $<0.05\%$ Cs was lost in the hydroxide–carbonate precipitate. A known aliquot of Ba carrier solution ($\sim$20 mg) was then added to the filtrate and the solution was allowed to stand for 90 min (about ten half-lives of Cs^{139}). Ba was isolated in the usual way (see below) and counted on methane flow β-proportional counters. The samples were monoisotopic, decaying with an 85-min half-life, since no other Ba isotopes grow from Cs on the time scale of the experiment.

2. Barium

The procedure used is based on that developed for separation of Ba from thermal neutron fission products.[54] Modifications were made in the experiments on 12.8-day Ba^{140}, due to the presence of spallation-produced isotopes of Ra in the sample.

For the determination of 85-min Ba^{139}, 5-min irradiations were performed and the samples were counted on β-proportional counters. For the mixture of 39-h Ba^{133m} and 29-h Ba^{135m}, the target was irradiated for

[54] L. E. Glendenin in *Radiochemical Studies: The Fission Products*, edited by C. Coryell and N. Sugarman (McGraw-Hill Book Co., New York, 1951), Nat. Nucl. Energy Ser., Vol. IV-9, p. 1657.

15 min, and the samples counted on a 1-in.-thick NaI(Tl) crystal. Because the two nuclides decay with unresolvable 39- and 29-h half-lives and 276- and 268-keV γ rays, respectively, recoil properties are reported only for the mixture. The two γ rays are resolved by a Li-drifted solid-state Ge detector, which makes possible the determination of the composition of the mixture. Because of low efficiency, it was impossible to measure the individual recoil properties. The results show the ratio of the cross section of Ba^{135m} to that of Ba^{133m} is 1.73.

The presence of isotopes of Ra is a serious problem only in counting Ba^{140}, where it may account for 15% of the total β activity of the sample 2 days after the end of irradiation.[8] Ra was separated from Ba by ion exchange based on a procedure of Power *et al.*[55] The solution containing Ba and Ra as nitrate was deposited on a column of 50–100 mesh Dowex 50, 8% crosslinked. The columns were approximately 25 cm long and 1 cm diameter. They were eluted with 0.4*M* ammonium citrate at a *p*H of 5.0. With a flow rate of approximately 6 drops/min, the Ba is eluted in 3 to 5 h. Tests using a Ra tracer showed that decontaminations averaging 1400:1 were achieved. Earlier experiments, in which the recoil properties of Ba^{140} were determined indirectly by La^{140} separations, yielded results in excellent agreement with the column separated Ba^{140}, although this procedure was abandoned in favor of the more efficient and less error-prone column separation.

3. Cerium

The chemical procedure used was essentially that of Glendenin *et al.*,[56] with slight modification due to the presence in the initial sample of large amounts of U or Al.

In about one-half of the Ce experiments, the x-rays of 140-day Ce^{139}, 32.5-day Ce^{141}, and 285-day Ce^{144} were counted on 1/8-in.-thick NaI(Tl) crystals beginning 1 month after a 2-h bombardment. The decay curves were analyzed by least-squares analysis after 15 months of counting. In the other experiments, the Ce samples were counted on a 1-in.-thick NaI(Tl) crystal, and the three γ-ray peaks occurring at 166, 145, and 134 keV for Ce^{139}, Ce^{141}, and Ce^{144}, respectively, were followed for 1 yr. While the peaks were not resolvable, the large change in the relative activities of the nuclides over a long period of time made analysis of the complex γ-ray peak possible. The agreement of results obtained from the two procedures was excellent, although the x-ray counting was discont nued when the thick crystals and associated multichannel analyzers became available.

After bombardments of about 15 min, 33-h Ce^{143} was chemically separated as above and counted by its characteristic 294-keV γ ray.

4. Rare Earths

The carrier for the element being studied in a given experiment was present in the target and catcher dissolving solutions. The procedure for the group separation was that of Nervik.[57] The separation of the individual rare earths (RE) was a modification of the procedure of Wolfsberg.[58]

The cation exchange column was approximately 65 cm long by 7.5 mm i.d. The resin used was Dowex 50, minus 400 mesh, 4% crosslinked. The eluting solution was 0.5*M* α-hydroxy-isobutyric acid, and the rare earths were added to the column in a minimum volume of nitric acid.

The fractions of an element under investigation were combined, generally taking only a narrow band at the yield peak, in order to lessen contamination by adjacent elements. The oxalates were precipitated, filtered, dessicated in vacuum at room temperature, and counted as $RE_2(C_2O_4)_3 \cdot 10H_2O$.

Lanthanum. The *p*H of the eluting solution was about 3.85 and elution took approximately 16 h. The samples were β^- counted, and there was no impurity found in any 40.2-h La^{140} experiments apart from small amounts of 4-h La^{141} activity initially present.

Praseodymium. Rare-earth chemistry was carried out as described above using an eluting solution buffered to a value of *p*H 3.90. At a flow rate of 9 ml/h, this sufficed to separate Pr in a maximum of 8–9 h. The $Pr_2(C_2O_4)_3 \cdot 10H_2O$ was counted with a 1-in.-thick NaI(Tl) crystal, and, after 12 h, on a β-proportional counter as well. Two-h Pr^{138} was counted via the 300-keV transition in its Ce daughter. Pr^{139} ($t_{1/2}$=4.5 h) was counted by the 511-keV annihilation radiation associated with positron decay, corrected for the 10% positron branch in the decay of 2-h Pr^{138}. Pr^{142} ($t_{1/2}$= 19.2 h) was counted both by its 1.58-MeV γ ray and as a component of the β-decay curve which includes 13.7-day Pr^{143}. Pr^{145} ($t_{1/2}$=5.9 h) was counted by both the 72 keV and the 670–740 keV γ rays.

Recent work[59] performed on 2-h Pr^{138} indicated that it is not formed in the decay of Nd^{138}, to which a half-life of 5 h has been assigned. The Nd^{138} decays to a short-lived excited state of Pr^{138} which, in turn, decays to Ce^{138}. This decay scheme was confirmed in these experiments by the absence of a γ-ray peak at 300 keV in samples in which Nd is first separated and Pr grows in.

Neodymium. In experiments investigating 3.3-day Nd^{140} and 11.1-day Nd^{147}, bombardments lasted for

[55] W. H. Power, H. W. Kirby, W. C. McCluggage, G. D. Nelson, and J. H. Payne, Anal. Chem. **31**, 1077 (1959).
[56] L. E. Glendenin, K. F. Flynn, R. F. Buchanan, and E. P. Steinberg, Anal. Chem. **27**, 59 (1955).
[57] W. Nervik, U.S. Department of Commerce Report No. NAS-NS-3020, 1961 (unpublished).
[58] K. Wolfsberg, Anal. Chem. **34**, 518 (1962).
[59] K. J. Gromow, A. S. Danagulyan, L. N. Nikityuk, V. V. Murav'eva, A. A. Sorokin, M. Z. Shtal', and V. S. Shpinel', Zh. Eksperim. i Teor. Fiz. **47**, 1644 (1964) [English transl.: Soviet Phys.—JETP **20**, 1104 (1965)].

1 h and the eluting solution was buffered to a pH of 3.8. Nd was eluted in 10–12 h and β decay of the samples was followed. For Nd experiments on the 5-h Nd isotope, irradiations of 15 min or less were performed and the eluting solution was buffered to 3.96. Nd was separated in 5 to 6 h and was β-counted as the oxalate.

During the course of this work, a question arose as to the existence of Nd^{138}, Nd^{139}, and Nd^{139m}. Little work[59–61] had been done on these nuclides since their discovery some 16 yr ago.[62] An attempt was made to study the recoil properties of Nd^{139} or Nd^{139m} by separating Nd, allowing the Pr to grow and decay, and, after several days, isolating Ce^{139} which decays with a well-known 166-keV γ ray accompanying electron capture. In several experiments, there was no evidence for Ce^{139} grown from a sample of separated Nd, although it was shown that Ce^{139} did indeed grow from Pr^{139} in the same experiment. The production cross section of Nd^{139} would have to be less than 1% of that of Pr^{139} to explain these results if the half-life of Nd^{139} is of the order of 5 h. The observation that Ce^{139} does not grow from Nd^{139} is consistent with that of Friedlander and co-workers,[63] who found no evidence for a 5.5-h–4.5-h complex decay curve in an isotope-separated mass-139 sample from the 29-GeV proton fission of U. These results are inconsistent with the conclusion of Gromow *et al.*[61] that the half-life of Nd^{139m} is 5.5 h. It should be noted, however, that Gromow *et al.* do not present evidence for the growth of Pr^{139} from Nd^{139m}. Recoil results for the 5-h isotope of Nd are therefore reported as Nd^{138} to which Gromow *et al.*[59] have also assigned a 5-h half-life. Because of the very low activity of Nd^{138} and the presence of 1.8-h Nd^{149}, the observed half-life of the Nd^{138} varied from 4 to 5.6 h in various runs.

Short-lived Nd^{141} ($t_{1/2}=2.5$ h), although presumably made in relatively high yield, decays by electron capture to the ground state of Pr^{141} with a branching ratio of 98%.[64] An attempt was made to count Nd^{141} by detecting the 2% positron branch, both by counting the β^+ and by counting its annihilation γ rays, but this attempt was not successful.

APPENDIX B: CHEMICAL AND COUNTING PROCEDURES; CHARGE DISPERSION EXPERIMENTS

The ratio of the production cross sections of $Cs^{139}(C)$ and $Ba^{139}(I)$ was determined by performing Cs chemistry as discussed in Appendix A, modified as follows. A measured aliquot of Ba carrier solution was present in the dissolving solutions and the hydroxide–carbonate precipitate was later analyzed for Ba. The activity of the two Ba samples, that grown in the filtrate, and that remaining in the precipitate, is related to cross sections of $Cs^{139}(C)$ and $Ba^{139}(I)$, respectively.

The ratio of the production cross sections of $Pr^{139}(C)$ and $Ce^{139}(I)$ was determined in two ways. First, aliquots were taken at timed intervals over 2 days and analyzed for Ce^{139} in order to compare its growth from the decay of 4.5-h Pr^{139} with the Ce^{139} initially present in the sample. Second, a sample, initially scavenged of Ce, was milked for Ce^{139} at intervals over 2 days, yielding the Ce^{139} growing from the 4.5-h Pr^{139}.

The ratio of the total production cross section of neutron-deficient nuclides to that of neutron-excess nuclides was determined by analysis of two aliquots of the target solution. The first was analyzed several hours after irradiation for cumulative Ba^{139}, and the second 4 days later for cumulative Ce^{139}. In both samples the same 166-keV γ-ray transition in La^{139} was counted, with correction for the 27% branching ratio from Ba^{139}.[64]

The Ce samples were counted on a solid-state Ge-Li detector which allowed for detection of the 166-keV peak of Ce^{139} in the presence of the 145- and 134-keV peaks of Ce^{141} and Ce^{144}, respectively. The samples were counted twice at an interval of about 4 months and half-lives of the three Ce nuclides were in agreement with literature values[64] within experimental error.

[60] N. A. Bonch-Osmolovskaya, B. S. Dzhelopov, O. E. Kraft, and Chou Yven-wa, Izv. Akad. Nauk SSSR Ser. Fiz. **25**, 826 (1961).
[61] K. J. Gromow, A. S. Danagolyan, A. T. Strigachev, and V. S. Shpinel', Izv. Akad. Nauk SSSR, Ser. Fiz. **27**, 1357 (1963).
[62] B. J. Stover, Phys. Rev. **81**, 8 (1951).
[63] G. Friedlander (private communication).
[64] C. M. Lederer, J. M. Hollander, and I. Perlman, in *Table of Isotopes* (Wiley-Interscience Inc., New York, 1967).